# Single-cell RNA sequencing reveals dysregulation of spinal cord cell types in a several spinal muscular atrophy mouse model

Junjie Sun [1#*], Jiaying Qiu [2#], Qiongxia Yang[1], Qianqian Ju[1], Ruobing Qu [4], Xu Wang[3], Liucheng Wu [3*], and Lingyan Xing [1*]

[1] Key Laboratory of Neuroregeneration of Jiangsu and Ministry of Education, Co-Innovation Center of Neuroregeneration, NMPA Key Laboratory for Research and Evaluation of Tissue Engineering Technology Products, Jiangsu Clinical Medicine Center of Tissue Engineering and Nerve Injury Repair, Nantong University, Nantong 226001, China.

[2] Department of Prenatal Screening and Diagnosis Center, Affiliated Maternity and Child Health Care Hospital of Nantong University, Nantong 226001, China

[3] Laboratory Animal Center, Nantong University, Nantong 226001, China

[4] Biomedical Polymers Laboratory, College of Chemistry, Chemical Engineering and Materials Science, Soochow University, Suzhou 215123, China

*To whom correspondence should be addressed at: Key Laboratory of Neuro regeneration of Jiangsu and Ministry of Education, Nantong University, 19 Qixiu Road, Nantong, Jiangsu Province 226001, China. Tel: +86 515506660626; Fax: +86 51365883602; Email: jjsun@ntu.edu.cn; hnwulc@ntu.edu.cn; xlyan011@163.com

**Abstract**

Although spinal muscular atrophy (SMA) is a motor neuron disease caused by the loss of survival of motor neuron proteins, there is growing evidence that lesions in nonmotor neuron cells are involved in SMA pathogenesis. Transcriptome alterations occurring at the single-cell level in SMA spinal cord are unknown. Here, we performed single-cell RNA sequencing of the spinal cord of a severe SMA mouse model, and characterized ten cell types as well as their differentially expressed genes. Using CellChat, we found that cellular communication between different cell types in the spinal cord of SMA mice is substantially reduced. A dimensionality reduction analysis revealed 29 cell subtypes and differentially expressed genes for each subtype. Among them, the most significant change in the SMA spinal cord at the single-cell level was observed in a subpopulation of vascular fibroblasts. This subpopulation was greatly reduced, which may be responsible for vascular defects in SMA mice and may lead to widespread reductions in protein synthesis and energy metabolism. This study is the first to report a single-cell atlas of the spinal cord of mice with severe SMA, providing new insights into SMA pathogenesis.

**Keywords：** spinal muscular atrophy; spinal cord; single-cell RNA sequencing; glial cell; fibroblast

## Introduction

Spinal muscular atrophy (SMA), a common lethal genetic disorder in children, is caused by mutations or deletions in the *survival of motor neuron 1* (*SMN1*) gene, which leads to failure in encoding the SMN protein [1]. Its pathology is characterized by motor neuron degeneration in the anterior horn of the spinal cord and necrosis of the neuromuscular junction [2]. Death in patients with SMA is due to respiratory failure caused by autonomic muscle denervation. Humans have a backup gene for *SMN1*, that is, *survival of motor neuron 1* (*SMN2*), which can produce a small amount of functional SMN proteins due to mis-splicing but cannot compensate for *SMN1* loss [3]. Direct supplementation of SMN proteins or the correction of *SMN2* splicing is the main approach used for SMA treatment. In recent years, three effective drugs for SMA treatment have been approved by the US Food and Drug Administration, namely Nusinersen, Risdiplam, and Abeparvovec-xioi. Nusinersen is an antisense oligonucleotide, and risdiplam is a small-molecule compound; these two drugs correct *SMN2* splicing; thus, increasing SMN protein levels. Abeparvovec-xioi is an adeno-associated viral vector–based gene therapy drug that increases SMN expression through the delivery of the full-length SMN coding sequence [4] [5; 6].

SMN is a functionally diverse housekeeping protein [7]. Its most well-understood function is to form a complex with the Gemin protein to participate in spliceosome assembly [8]. Another essential function of SMN is to participate in messenger RNA transport in motor neuron axons [9]. However, no SMN downstream molecule has been identified so far that causes motor neuron degeneration due to splicing errors or altered localization. SMN influences the SMA condition in a dose-dependent manner. In general, the more the copies of the SMN2 gene, the milder the clinical phenotype of SMA. In addition, several modifiers affect the clinical phenotype of patients with SMA. Patients carrying the c.859G>C mutation on exon 7 and A-44G mutation on intron 6 of SMN2 had a mild phenotype; the c.859G>C mutation creates an SF2/ASF-dependent exonic splice enhancer, and the A-44G mutation disrupts the HuR-dependent intronic splicing silencer [10; 11]. Furthermore, the overexpression of plastin 3 and neurocalcin delta can improve the clinical phenotype of patients with SMA [12; 13].

Numerous studies have proposed that in SMA, motor neurons undergo non-cell-autonomous death. Specific depletion of SMN in motor neurons causes limited dyskinesia rather than complete SMA [14]. Although a specific increase in SMN protein in motor neurons improves the pathological features and motor functions of SMA mice, the improvement in mouse lifespan is limited [15]. Among the cell groups in the central nervous system (CNS), glial cells are one of the most abundant, and their main function is to support the homeostasis of the spinal cord and nourish neurons. Therefore, theoretically, glial cells are the most likely to be involved in the non-cell-autonomous death of motor neurons. Astrocytes in SMA undergo morphological and functional changes, reducing communication with motor neurons by affecting calcium homeostasis, microRNA formation, and protein secretion [16; 17; 18; 19]. Surprisingly, SMN-specific supplementation in astrocytes did not prevent motor neuron death but increased the lifespan of SMA mice [20]. In addition, other cell types in the spinal cord, such as vascular, are impaired [21]. Indeed, the spinal cord is a highly heterogeneous and complex tissue, and different cell types or subtypes may play different roles in SMA pathogenesis. Therefore, an objective and comprehensive understanding of the genetic alterations of each cell type in the SMA process and the effects on neurons is essential.

Several studies have used transcriptomics to explore SMA pathogenesis, revealing numerous gene expression and splicing alterations in the tissues of SMA mice or patient cells [22; 23; 24; 25; 26; 27; 28]. However, these studies have not identified which cell types in the SMA spinal cord are diseased and what genetic changes occur to these cell types. Single-cell RNA sequencing (scRNAseq) is an emerging technique suitable for the analysis of cellular heterogeneity. This technique has uncovered disease-specific cell populations and genes that have never been reported before in Alzheimer disease (AD), Amyotrophic lateral sclerosis (ALS), Multiple sclerosis (MS), Parkinson's disease (PD), Huntington’s disease (HD), and other diseases, providing new insights into these neurodegenerative diseases with unclear mechanisms [29; 30; 31; 32; 33; 34].

We performed scRNAseq of the intact spinal cords of severe SMA mice and heterozygous mice. A total of 22,155 cells were analyzed, and they were classified into 10 cell types, including oligodendrocyte precursor cells (OPCs), oligodendrocytes

(OLs), committed OL precursors (COPs), neurons, schwann cells, blood cells, astrocytes, microglia, ependymal cells, and vasculature. We analyzed cell-type-specific differentially expressed genes (DEGs) and cell–cell communication between the different cell types. In addition, we identified cell subtypes and disease-specific genes for each subtype. Finally, we found that fibroblasts are substantially reduced in SMA mice, which emphasizes the significance of vascular defects in SMA pathogenesis.

## Results

### scRNAseq and cell-type identification of the spinal cords of SMA and control mice

For scRNAseq, we selected type I Taiwanese SMA mouse models that were 4 days postnatal (P4). These mice exhibited severe SMA with a lifespan of approximately 10 days [35]. Studies have stated that treatment with Nusinersen at 1–3 days postnatal instead of 5–7 days postnatal can improve the lifespan of these mice, suggesting that P4 is a turning point in the deterioration process of SMA mice [36].

To explore disease-specific cell types and cell-type-specific DEGs, we first constructed a single-cell atlas. The spinal cords of three SMA mice ($Smn^{-/-}$, $SMN^{2tg/0}$) at P4 were pooled as one sample for single-cell digestion, and heterozygous mice ($Smn^{+/-}$, $SMN^{2tg/0}$) from the same litter were used as controls. Individual cells from both samples were subjected to scRNAseq based on a 10× Genomics protocol. After quality-control filtering, 8887 control cells and 13,268 SMA cells were used for subsequent analysis, with an average median of 1933 genes per cell. To analyze global gene expression changes in the spinal cord, we constructed a bulk-seq atlas from the spinal cord tissues of SMA and heterozygous mice of the same age. Bulk-seq detected >20000 genes in total.

The uniform manifold approximation and projection (UMAP) method was used for the visualization and classification of all cells. The cells were divided into 16 clusters **(Fig. 1A)**. Based on the expression of known CNS cell-type-specific genes [29], they were mapped into 10 cell types: astrocytes (cluster 0), microglia (clusters 1 and 12), OPC (clusters 2, 4, and 7), COP (cluster 3), OL (cluster 11), neuron (cluster 16), ependymal cells (clusters 11 and 15), vasculature (clusters 6, 13, and 9), blood cells

(clusters 5 and 8), and Schwann cells (cluster 14) **(Fig. 1 B sup-1 A, B)**. OPCs were the most abundant, accounting for 22.97% of the total cells, whereas the proportion of neurons was the lowest, accounting for 0.46% of the total cells **(Fig. 1C)**. No significant difference was observed in the overall cell proportion between SMA and control mice **(Fig. 1D, E)**. The proportion of neurons and ependymal cells in SMA mice was slightly higher than that in control mice, and the proportion of blood cells in SMA mice was slightly lower than that in control mice **(Fig. 1E)**. In this study, the number of neuronal cells which expressed Meg3, Tubb3 and Snhg11 is too small to determine whether this is a motor neuron or not [37; 38; 39; 40; 41]. This approach from single cell suspension may result in neuronal loss.

**DEGs and functional analysis of SMA spinal cord cell types**

We focused on cell type-specific DEGs in SMA and control mice. Approximately 5000–7000 genes were detected in most of the cell types aforementioned, except for blood cells, where only 2008 genes were detected **(Sup 2A)**. According to log fold change (logFC) $\geq 0.2$ and $p < 0.01$, the DEGs of each cell type were defined, with neurons, vasculatures, and COPs having the highest number of DEGs (960, 343, and 373, respectively) and OPCs, microglia, and ependymal cells having the lowest number (45, 50, and 52, respectively) **(Fig. 2A and Sup File 1)**. Notably, the number of downregulated genes was much larger than that of upregulated genes in cell types other than blood cells, and this trend of predominantly downregulated expression was consistent with the results of bulk-seq **(Fig. 2B)**.

Although neurons had the highest number of DEGs, the fold change was small **(Fig. 2C)**. The most differentially upregulated gene is Apoe, a marker gene of microglia that has been associated with neurodegenerative diseases, such as AD [42]. Downregulated genes with the largest fold in neurons are Hbb-a1, Hbb-bs, and Hbb-bt, which are genes encoding hemoglobin, and their homolog Hbb-b1 was downregulated in another more modest SMA mouse Smn2B/− [43]. The X inactive specific transcript (Xist), which is downregulated in most cells, is a major regulator of mammalian X chromosome inactivation and is sex-specific. In the bulk-seq data, the expression of this gene was generally higher in female mice than in male mice **(Sup 2B)**. A total of

15 genes were downregulated in vasculatures at >2-fold. From large to small, they were Timp1, Col3a1, Mfap5, Col1a2, Col1a1, Ccl7, Ccl2, Lgals1, S100a6, Ly6a, Bgn, Rarres2, Dcn, S100a10, and Cxcl1 **(Fig. 2D)**. Among them, Col3a1, Mfap5, and Dcn are vascular fibroblast marker genes, suggesting that the differences in vasculature mainly come from fibroblasts. Ccl7 and Ccl2 encode chemokines and mediate axonal growth as downstream molecules of axonal SMN [44].

Using the Gene Ontology (GO) database, the biological processes (BP) of the DEGs of each cell type were analyzed. DEGs in neuronal cells were mainly enriched in intracellular molecular localization; Schwann cells, astrocytes, and OL lineage cells were mainly enriched in nervous system development and neurogenesis; blood cells were enriched in protein synthesis; microglia were enriched in extracellular stimulus response and defense response; vasculature cells were enriched in altered extracellular components and cell migration **(Fig. 2E)**. Most of the GO terms of these non-neuronal cells were associated with the cell membrane or extracellular matrix, suggesting that cellular communication in the SMA spinal cord may have been altered.

**Effects of SMN deletion in different cell types are heterogeneous**

We next performed an integrated analysis of data obtained from scRNAseq and bulk-seq. After comparing DEGs in cell types with bulk-seq and counting the number of overlapping genes, we found that few DEGs appeared in three or more cell types, suggesting that SMN deletion caused different gene expression changes in different cell types **(Fig. 2F)**. Only one DEG, Hbb-bt, was universally down-regulated in bulk-seq and scRNAseq, and another DEG, Hbb-a1, was downregulated in all cell types except COP **(Sup 2C)**.

The expression differences of Hbb-bt and Hbb-a1 are not large in blood cells but large in OL cells **(Sup 2D)**. Tmsb10 was the only upregulated gene in multiple cell types, with the highest expression in neurons and vasculature and with the greatest difference in astrocytes **(Sup 2D)**. The change trend of most genes in cell-type-specific DEGs was consistent with bulk-seq, and vasculature matched the highest number of DEGs with bulk-seq **(Sup 2C and Fig. 2G)**. The Kyoto Encyclopedia of Genes and Genomes (KEGG) pathway analysis for DEGs showed that two pathways, amino acid

biosynthesis and phagocytosis, were significant in bulk-seq and six cell types; two pathways, fatty acid degradation and peroxisome functions, were significant in bulk-seq alone and failed to enrich in all cell types **(Sup 2E)**. Although OPCs have numerous DEGs, only one pathway, that is, phagocytosis overlaps with bulk-seq. The differential pathways of vasculature and microglia were the most similar to bulk-seq, with overlaps in >50% of the pathways **(Sup 2E)**.

Our results suggest that the effects of SMN on different cell types are heterogeneous; bulk-seq cannot sufficiently determine gene expression changes across cell types; bulk-seq results are the most similar to scRNAseq results for vasculature.

**Cell–cell communication is reduced in the spinal cord of SMA mice**

We used CellChat to analyze the communication network among spinal cord cells of control and SMA mice. On the basis of the ligand–receptor pair, CellChat provides two analysis methods, one is mainly for secreted signaling interactions (SSIs), and the other is biased toward cell–cell contact interactions (CCIs) [45]. Schwann and blood cells were removed due to their localization in the peripheral nervous system and too few genes detected. The overall CCIs in the spinal cord of SMA mice were significantly reduced, with a 50% and 30% reduction in the number and strength of interactions, respectively **(Fig. 3A)**. The cell types with the most significant reduction in CCIs, both in number and strength, were OPCs and COP cells, and the cell type with the least significant reduction was microglia **(Fig. 3B, C)**. The interactions among OPCs, COPs, and neurons decreased the most significantly **(Fig. 3B, C)**. Overall, SSIs in the spinal cord of SMA mice were reduced by 31% and 23% in terms of the number and strength of interactions, respectively **(Fig. 3D)**. The most significant reduction in the number of interactions was in vasculature, and the most significant reduction in the strength of the interactions was in OPCs and COPs **(Fig. 3E, F)**. The number and strength of SSIs decreased across most cell types in SMA but increased in microglia **(Fig. 3E, F)**, which may be related to microglia activation reported earlier [46].

We focused on alterations in neuronal communication with other cell types. Eight and three SSI-based pairings decreased and increased in SMA, where ptn-sdc3 was detected only in SMA but not in controls **(Fig. 3G)**. Nine and three CCI-based pairings

decreased and increased in SMA, respectively **(Fig. 3H)**. Sema–Plxna and Ncam–Licam pairs are expressed specifically in controls and are absent in SMA. Nrxn–Nlgn3 and Mpzl1–Mpzl1 were present only in SMA and absent in controls **(Fig. 3H)**.

**Identify cell subtypes and their DEGs**

We next subdivided each cell type into subtypes. Astrocytes were divided into five clusters after dimensionality reduction **(Fig. 4A)**. AS-2 had the characteristics of progenitor cells because the markers of these cells contain cell cycle–related genes such as Cdca8 and Stmn1 and were significantly enriched in the cell cycle pathway **(Sup 4A, B)**. The marker genes of AS-1 and AS-4 were mainly enriched in the ribosome; hence, they were defined as mature astrocytes. The main difference between the two subtypes was that the main function of AS-1 was biased toward intracellular signal transduction, whereas AS-4 had microglia characteristics, with high expression of C1qa, C1qb, and Tyrobp **(Sup 3A, B)**. AS-3 had blood cell characteristics. AS-0 was the cluster with the highest number of cells, but it cannot be functionally defined due to a lack of signature genes.

Ependymal was dimensionally reduced into two clusters, with Ep-0 favored for secretion and Ep-1 favored for metabolism **(Fig. 4B, Sup 3C, D)**.

Microglia were classified into six subtypes **(Fig. 4C)**. Of these, MG-0 was the most abundant, expressing most genes associated with microglial homeostasis, such as Cx3cr1, Trem2, and P2ry12, but no specific gene was highly expressed. Markers of the MG-1 subtype can be significantly clustered in the metabolic pathway, defined as the metabolic microglia. The characteristic genes of MG-2 were Birc5, Cdca8, and Stmn1, and their functions are significantly enriched in the cell cycle and DNA replication pathways, which were defined as dividing microglia. MG-3 cannot be functionally defined due to too few marker genes. MG-4 specifically highly expresses Pf4, F13a1, and Lyve1, and marker genes can be significantly enriched in the phagocytosis and endocytosis pathways, which were defined as phagocytic microglia. The markers of MG-5 included S100a11 and S100a6, which were significantly clustered in cell migration and cell adhesion and were defined as migrating microglia **(Sup 3E, F)**.

Eleven OL lineage subtypes were identified **(Fig. 4D)**. OL-5 highly expressed Mag,

Mbp, and Mog, which were typical markers of myelinating OL. Markers of OL-3 were significantly enriched in the axon guidance pathway, overlapping with OL-5, but the expression of myelin markers was low, and hence, it is defined as a nonmyelinating mature OL. OL-1 specifically expressed Bmp4 and Nkx2–2, which was defined as COPs. OL-2, OL-4, OL-6, and OL-10 can be enriched with the cell cycle pathway and are defined as OPCs, of which OL-4 and OL-6 were OPCs with a strong dividing ability. Although OL-0 cannot be enriched with the cell cycle pathway, this subtype highly expressed OPC markers, such as Pdgfra and Cspg5, and was also defined as OPCs **(Sup 3G, H)**.

Vasculatures contained five subtypes **(Fig. 4E)**. Vas-0 and Vas-4 had overlapping markers, and both highly expressed Cldn5, Pglyrp1, and Egfl7, which were defined as endothelial cells. The marker genes of Vas-1 were Rgs5 and Myl9, which were significantly enriched in the thermogenesis and oxidative phosphorylation pathways and were defined as pericytes. Both Vas-2 and Vas-3 expressed Col3a1 and Dcn specifically and had similar functions, and were the subtypes of perivascular fibroblasts. The difference between the two was that markers of Vas-2 but not Vas-3 were significantly enriched in inflammation-related pathways such as interleukin-17 and tumor necrosis factor **(Sup 3I, J)**.

We compared the DEGs for each cell subtype in SMA and control mice. Vas-2 has 1362 DEGs, which is considerably more than that in other subtypes, suggesting that Vas-2 may be the most severely defective cell subtype in the spinal cord of SMA mice **(Fig. 4F)**. MG-5, OL-5, OL-10 and Vas-3 also have more DEGs, 549, 460, 388 and 397, respectively **(Fig. 4F, Sup File 2)**.

**Altered gene expression of glial cell subtypes in the SMA spinal cord**

We first analyzed changes in cell numbers of major glial cells. No significant differences in cell numbers were observed in the subpopulations of the OL lineage and astrocytes in SMA compared with controls **(Sup 4A, B)**. But, the cell number of the migrating microglia MG-5 was reduced by approximately two-third in SMA mice compared with control mice **(Sup 4C)**. Although this population was the microglia population with the largest number of DEGs, neither the fold nor the p-value of the

changes in DEGs was significant **(Fig. 5A)**. Functional analysis revealed that downregulated genes in MG-5 in SMA were mainly associated with immune system response, translation, and RNA splicing, and upregulated genes were not functionally significant **(Fig. 5B)**.

OL-5 was a subtype of OL lineage with the most DEGs of which the most significant were Apoe and Fabp7 **(Fig. 5C, D)**. These two genes were highly expressed in astrocytes and microglia **(Sup 4D)**. Apoe encodes a member of the apolipoprotein A1/A4/E family, and mutations in this gene are the strongest genetic risk factors for AD [47]. Fabp7 encodes a member of the fatty acid-binding protein family, which can bind to fatty acids, a crucial component of myelin [48; 49]. The BP analysis of DEGs revealed that downregulated DEGs were mainly related to protein synthesis, whereas upregulated DEGs were mainly concentrated in myelination-related pathways **(Fig. 5E)**. Consistently, the cellular component analysis of DEGs revealed that downregulated and upregulated genes were mainly localized to the ribosome and myelin sheath, respectively **(Fig. 5F)**.

OL-5 is a myelinating OL subtype, and the increased myelin-forming capacity of this subtype in SMA is worthy of reconfirmation. We performed a pseudo timeline analysis of OL lineage in SMA and control mice**,** no significant difference was observed in their OL lineages **(Sup 4E, 4F)**. The OL-5 of SMA was more mature than that of controls, which was consistent with the results of the BP analysis **(Sup 4F, G)**. In addition, OL-0, OL-2, OL-4 and OL-10 cell populations tended to be more mature, whereas OL-1 and OL-3 tended to be immature in SMA **(Fig. 5G)**. Our results suggest that SMA myelinating OL has reduced protein anabolism, but this does not appear to affect their myelinating function.

**Subpopulation of perivascular fibroblasts was drastically reduced in SMA spinal cords**

The Vas-2 subtype in SMA was drastically reduced **(Fig. 6A)**. Both Vas-2 and Vas-3 are fibroblast subpopulations, and SMA selectively depletes Vas-2 without affecting the number of Vas-3 cells **(Fig. 6A, B)**. Most fibroblast markers are downregulated in vas-2, such as Col3a1, Col1a1, Dcn, and Fn1 **(Fig. 6C)**. The gene with the largest fold

differential expression was Col3a1, which was downregulated by nearly 4-fold **(Fig. 6C, D)**. In addition, Rarres2, the gene encoding the angiogenesis regulator Chemerin, was also downregulated by >2-fold in this cell population [50] **(Fig. 6C, E)**. Notably, these DEGs that were significantly altered in the two fibroblast subtypes Vas-2 and Vas-3 overlapped slightly, again indicating that the effect of SMN deletion was cell-type specific **(Fig. 6F)**.

Somers et al. showed that both humans and mice with SMA have vascular defects that lead to hypoxia, which may be one of the reasons for motor neuron death [21]. Our findings further suggest that the cause of vascular defects may be the depletion of a fibroblast subpopulation. We performed immunofluorescence experiments to confirm this crucial finding. Pecam1/CD31 and Col3a1 were used to label blood vessels and fibroblasts, respectively. The results showed that CD31 and Col3a1 were co-localized, suggesting that vascular endothelial cells and fibroblasts coexisted spatially **(Fig. 6G)**. After statistics, the expression of both CD31 and Col3a1 was reduced in the spinal cord of SMA mice at P4. This suggest the reduction in Vas-2 may contribute the vascular defects [21]**(Fig. 6G, H)**.

We observed reductions in pathways related to energy metabolism and protein synthesis that are widespread across cell types as well as whole of SMA **(Fig. 6I, Sup 5)**. The inhibition of these two pathways is a direct consequence of cellular hypoxia. Thus, we can hypothesize that due to the depletion of one fibroblast subtype, the oxygen transport capacity of blood vessels is reduced, which leads to a hypoxic state of various cell types, causing a series of pathological changes in SMA.

## Discussion

Although motor neuron degeneration is a hallmark feature of SMA, increasing evidence suggests that SMA is a systemic disease caused by SMN protein deficiency [51]. Hua et al. confirmed that SMA is a non-cell-autonomous defect of motor neurons caused by non-motor neuron cytopathies [52]. However, the cell types in the spinal cord affected by SMA and the extent of involvement of the SMN protein in the different cell types are unexplored. Here, we used scRNAseq and bulk-seq to sequence the genes in

the spinal cords of severe SMA mice on P4 and attempted to fill the aforementioned knowledge gap.

In particular, we defined 10 cell types, including OPCs, OLs, COPs, neurons, Schwann cells, blood cells, astrocytes, microglia, ependymal cells, and vasculatures, and compared their DEGs caused by SMA. A key advancement of this study compared with the extensive spinal cord transcriptome data reported previously is that in our study, transcriptome data are not perturbed by other cell types [22; 53; 54; 55; 56; 57]. Several studies have used laser capture microdissection to isolate motor neurons and glial cells, which greatly improved the purity of individual cell types, but this still did not completely rule out interference from other cell types [23; 25; 43; 58]. DEGs are different in almost every cell type, but whether this difference is caused by SMN selection is unknown. The downregulation of hemoglobin genes (Hba-a1 and Hbb-bt) was observed in most cell types and bulk-seq. Hemoglobin is known for binding oxygen in red blood cells, but they are also present in neurons and glial cells [59; 60]. Studies have confirmed that the downregulation of hemoglobin gene expression is associated with neurodegenerative diseases, such as AD and MS [61; 62]. In the spinal cord of SMAΔ7 mice, the hemoglobin-encoding genes Hbb-b2 and Hbb-b1 were downregulated by 2.6-fold at 7 days after birth [54]. Significant recovery of hemoglobin subunit alpha was observed in the cerebrospinal fluid of type 1 SMA patients treated with Nusinersen [63]. Hemoglobin-encoding genes were not significantly altered in SMN knockout Hela cells, suggesting that they are not direct downstream molecules of SMN and may be the result of reduced cellular oxygen metabolism [22].

Bulk-seq and microarray data of type I Taiwanese SMA mice spinal cord showed that only a few genes were altered in presymptomatic mice (P1), whereas numerous gene expression changes were observed in the late stage of the disease (P5) [22; 55]. P4 is considered an intermediate state in disease development and has received less attention before. Both our scRNAseq and bulk-seq showed that the number of downregulated genes was much greater than that of upregulated genes in the P4 spinal cord, a pattern different from that of P5. The cell division pathway and axon guidance genes were significantly downregulated in the P5 spinal cord, which was not observed

in the P4, indicating that SMA pathogenesis undergoes great physiopathological changes from the middle stage to the late stage [22]. Most of the down-regulated pathways in the P4 spinal cord are metabolically related, consistent with the widespread metabolic dysregulation of SMA that has been demonstrated [64].

Normal communication between the various cell types of the spinal cord is required for the maintenance of neuronal structure and function, particularly during development [65]. Dysregulation of intercellular communication leads to SMA [66]. The analysis by using CellChat revealed that intercellular communication in the spinal cord of SMA mice was reduced both in number and intensity. One of the most altered cell types is astrocytes. A study based on *in vitro* culture systems demonstrated defective interactions between astrocytes and motor neurons in SMA [19]. Moreover, great alterations have been noted in the communication between the cell types OPC and COP, but so far, no study has confirmed whether this affects SMA. We identified several ligand–receptor pairs differentially expressed in SMA and control mice. Ncam and L1cam are downregulated in SMA patients or cell models of motor neuron disease, consistent with our results [67; 68; 69]. Although whether most of these ligand–receptor pairs play a role in SMA pathogenesis is unclear, they still provide potential topics for follow-up research.

Numerous studies have focused on transcriptome alterations in SMA motor neurons. In addition to the aforementioned laser capture microdissection, several studies have analyzed the transcriptome of motor neurons produced from SMA patient-derived induced pluripotent stem cells. Although both Giacomo P Comi's team and Lee L Rubin's team obtained Hb9 positive cells with high purity, the DEGs and pathways found in the two studies were not the same due to different sources of its cells and different induction methods [26; 27; 28]. Motor neurons themselves have abundant subtypes [70]. Ling et al. found that in mice with severe SMA, in the late stage of the disease, motor neurons do not innervate all muscles equally but selectively denervate some of them (e.g., axial muscles and appendicular muscles) [71]. Another study revealed that SMNs have different roles in maintaining the integrity of central and peripheral synapses [72]. Thus, different neuron types may play different roles in SMA.

However, only a small number (0.46%) of neuronal cells were identified in this study, which is not enough to distinguish whether they belong to motor neurons and to which subtype, which is a drawback of this study. In the future, scRNAseq of neurons sorted through flow cytometry can address this knowledge gap.

Microglia are immunocompetent cells of the CNS [73]. Significant microglia activation was observed in SMAΔ7 mice with late disease (after 10 days after birth) but not in the early and middle stage (before 7 days after birth) [74] [46; 75]. Aleksandra Vukojicic et al. reported that microglia leads to abnormal spinal cord motor circuits in SMAΔ7 mice by activating the canonical complement pathway [76]. However, this phenomenon was not evident in the early stage of the disease (P4), and pharmacological inhibition of the complement pathway had limited lifespan improvement in SMA mice. Thus, microglial activation is a consequence rather than a cause of SMA. No reports are available regarding microglia activation in the spinal cord of type I Taiwanese mice. Our data divided microglia into six subtypes, among which the migrating microglia MG-5 was the most divergent between SMA and control mice, possibly the subtype directly affected by SMA.

Astrocytes are one of the most abundant cell types in the CNS and play crucial roles in physiological processes such as maintaining ion homeostasis, nourishing and protecting neurons, and developing synapsis and plasticity [77]. Supplementation of SMN specifically to astrocytes doubles the lifespan of Δ7 SMA mice, suggesting that astrocytes can affect the severe form of SMA [20]. Our scRNAseq data revealed that a reactive astrocyte subtype with stronger “ribosomal” activity, AS-4, was significantly different between SMA and control mice. The marker genes of AS-4 are C1qa, C1qb, and Tyrobp, and these genes have the characteristics of microglia. The team of Ben A Barres reported that a subpopulation of reactive astrocytes with a highly upregulated expression of many classical complement cascade genes, called A1, is similar to AS-4 identified in this study [78; 79]. A1 cannot maintain synaptic function, loses phagocytic ability, and is highly neurotoxic [78]. This subtype is present in various neurodegenerative diseases such as HD, AD, PD, MS, and ASL and is induced by normal aging [78; 80]. Our scRNAseq data suggest that this subtype is also present in

SMA and may play a role in SMA.

The traditional view is that OLs are myelinating cells in the CNS. Many new functions of OL lineages beyond myelination have been gradually elucidated, such as providing metabolic support to neurons and regulating water and ion homeostasis [81]. Whether OL lineages are involved in SMA pathogenesis is controversial. O'Meara et al. found that OL growth, migration, differentiation, and myelination were not affected in severe SMA mice ($Smn^{-/-}$, $SMN2^{+/+}$) [82]. However, Kazuki Ohuchi et al. found that the OL lineage was impaired in Δ7 SMA mice [83]. Our data show that the subtype of OL lineages that is most affected by SMA is the myelinating OL subtype, OL-5, whose myelinogenic function is not affected. Therefore, our data support that the myelinating function of OL in SMA is not abnormal, consistent with the conclusions of O'Meara et al. Compared with SMAΔ7 mice, type 1 Taiwanese SMA mice ($Smn^{-/-}$, $SMN2^{2TG/-}$) have a closer genetic background and lifespan to the ($Smn^{-/-}$, $SMN2^{+/+}$) mice used by O'Meara et al, which may be one of the reasons for the similar conclusions. Notably, the protein synthesis pathway was significantly reduced in OL-5, suggesting that the myelin sheath of SMA is more inclined to remain in a quiescent state. Furthermore, the aforementioned COP cells and OPCs are cell types with the most pronounced reduction in cellular communication in SMA. Therefore, it cannot be ruled out that OL lineage has lesions other than myelination in SMA.

vasculature is a crucial source of material and energy metabolism in the CNS, and their integrity is key to ensuring the normal function of the spinal cord. Structural and functional abnormalities of the vasculature are widespread in neurodegenerative diseases [84; 85]. Vascular defects have been identified in SMA patients and mouse models through morphological observation [21; 86; 87; 88]. Our data demonstrated that two fibroblast subpopulations were significantly altered in SMA, with one subpopulation decreasing in numbers off a cliff. Our findings refine the affected vascular subpopulations, which have crucial implications for exploring the cellular targets of SMA. Fibroblasts are a group of cells that attach to the outer walls of blood vessels and are found in all blood vessels except capillaries [89; 90; 91]. The well-known function of fibroblasts is to participate in fibrotic scar formation after spinal cord

injury [92]. The fibroblast markers Col3a1 and Dcn are greatly upregulated after spinal cord injury [93]. Andrew C Yang et al. pointed out that fibroblasts may be involved in ion and amino acid transport in the CNS [94]. In addition, fibroblasts transmit signals through the bloodstream, affecting the progression of neurodegenerative diseases. ALS patients in whom fibroblast protein product accumulates in perivascular space have shorter survival times [95]. In fact, as one of the indispensable components of the vasculature, the function of fibroblasts is somewhat unclear, and there may be unknown functions in SMA [85].

We observed widespread inhibition of energy metabolism and protein synthesis pathways across cell subtypes. Alterations in these pathways may be another manifestation of morphological and functional defects in mitochondria in SMA mouse motor neurons [96]. Somers et al. demonstrated that the spinal cord of SMA mice has a defect in the blood–spinal cord barrier with significant functional hypoxia [21]. The weakened interaction between vascular and CNS cells in our results also demonstrates to some extent that an abnormal blood vessel structure may lead to decreased material exchange with CNS cells, thereby affecting spinal cord function. A possible future direction is to determine why fibroblasts are sensitive target cells for SMA and their specific role in SMA.

In summary, this study provides the first single-cell atlas of SMA. Through scRNAseq, we identified the disease-specific DEGs of each cell type and subtypes of SMA spinal cord and found that the decrease in the number of vascular fibroblasts was the most severe at the single-cell level. These never-before-reported findings provide new insights into SMA pathogenesis.

## Materials and Methods

### Animal management

The experimental animals in this study were housed in the Specific Pathogen Free barrier provided by the Animal Center of Nantong University under the following conditions: temperature (22°C ± 2°C), humidity (60% ± 5%), and light of Alternate dark/light for 12 hours. Animal experiments were approved by the Animal Ethics

Committee of Nantong University and followed the International guidelines (NIH) for the Care and Use of Laboratory Animals (No.2150409).

**Generation of transgenic mice**

The Taiwanese SMA mice used in this study was a gift from Professor Hua Yimin at Soochow University and was originally purchased from the Jackson Laboratory (FVB.Cg-Smn1tm1HungTg (SMN2)2Hung/J, stock number 005058) [35; 97]. There are two genotypes of this mouse, severe ($Smn^{-/-}$, $SMN^{2tg/0}$) and mild ($Smn^{-/-}$, $SMN2^{2tg/2tg}$). Severe and control mice ($Smn^{+/-}$, $SMN2^{tg/0}$) were sequenced in this project, generated by crossing Het knockout mice ($Smn^{+/-}$) with mild Taiwanese mice ($Smn^{-/-}$, $SMN2^{2tg/2tg}$). Genotyping of tail-end tissue from newborn mice was performed using the method described in One step mouse genotyping kit (PD101-01, vazyme, nanjing, china). A Primer pair (F: 5'-AGCCTGAAGAACGAGATCAGC-3', R: 5'-GTAGCCGTGATGCCATTGTCA-3') was used to detect mutant or K/O mouse Smn1 locus. A primer pair (F: 5'-AAGTGAGAACTCCAGGTCTCCTG-3', R: 5'-TTCACCGTGTTAGCCAGGATGGTC-3') was used to detect the human SMN2 gene.

**Preparation of single-cell suspension**

Whole spinal cords were obtained from transgenic mice, and the spinal cords were stripped according to established methods and placed in ice-cold phosphate-buffered saline (PBS) [98]. The tissue was minced and dissociated with 0.25% trypsin in a centrifuge tube for 30 min at 28 °C, followed by 1 mg/mL collagenase II for 20 min, with gentle mixing every 10 min. The enzymatic reaction was terminated through the addition of 10% fetal bovine serum (FBS). The sample was filtered using a 70 μm strainer to obtain a single-cell suspension.

**scRNAseq**

Using single-cell 3 'Library and Gel Bead Kit V3 (10× Genomics, 1000075) and Chromium Single Cell B Chip Kit (10× Genomics, 1000074), the cell suspension (300–600 living cells per microliter determined by Count Star) was loaded onto the Chromium single cell controller (10× Genomics) to generate single-cell gel beads in the emulsion according to the manufacturer's protocol. In short, single cells were suspended in PBS containing 0.04% bovine serum albumin (BSA). Approximately

6000 cells were added to each channel, and the target cell recovered was estimated to be approximately 3000 cells. Captured cells were lysed, and the released RNAs were barcoded through reverse transcription in individual GEMs. Reverse transcription was performed on an S1000TM Touch Thermal Cycler (Bio Rad) at 53 °C for 45 min followed by 85 °C for 5 min, and incubated at 4 °C. The complementary DNA (cDNA) was generated and then amplified, and the quality was assessed using an Agilent 4200. According to the manufacturer's instruction, scRNAseq libraries were constructed using Single Cell 3' Library and Gel Bead Kit V3. The libraries were finally sequenced using an Illumina Novaseq6000 sequencer with a sequencing depth of at least 100,000 reads per cell with a pair-end 150 bp reading strategy (performed by CapitalBio Technology, Beijing).

**Bulk-seq**

The total RNA of spinal cord tissue was extracted through the Trizol method and sent to Vazyme Company (Nanjing, China) for sequencing. Briefly, ribosomal RNA removal was performed first. Using ribosomal-depleted RNA and random hexamers to synthesize one-stranded cDNA, and then we added buffer, deoxynucleoside triphosphates, and enzymes to synthesize two-stranded cDNA. Double-stranded DNA was purified using VAHTS™ DNA Clean Beads, followed by end repair, A-tailing, and the ligation of sequencing adapters. The cDNA strand containing U was degraded by the uracil-DNA glycosylase enzyme, and finally, PCR enrichment was performed; the PCR product was purified with VAHTS$^{TM}$ DNA Clean Beads to obtain the final strand-specific cDNA library. Illumina HiSeq sequencing was performed after the library was qualified for quality control.

**RNA-seq data processing**

First, the raw data of bulk-seq was converted into high-quality clean reads. Then, hisat2 [99] was used to align the clean reads to the reference genome of *Mus musculus*. Fragments per kilobase of exon per million mapped fragments (FPKM) expression values of genes were quantified using cufflinks software [100].

For the 10× genomics data, the Cell Ranger Single-Cell toolkit (version 3.0.0) provided by 10× genomics was applied to align reads and generate the gene-cell unique

molecular identifier (UMI) matrix for each sample (https://support.10xgenomics.com/single-cell-gene-expression/software/downloads/latest). The read data were mapped using the corresponding *Mus musculus* reference genome. Different samples were merged using the cellranger aggr function. The obtained raw_feature_bc_matrix was loaded, and Seurat R package (v 3.2.2) was further used for downstream analyses [101]. Further quality control was applied to cells based on three metrics step by step, including the total UMI counts, number of detected genes, and proportion of mitochondrial gene counts per cell. Specifically, cells with <200 detected genes and those with a high detection rate (10%) of mitochondrial gene expression were filtered out. To further remove potential doublets in our data, cells with the number of detected genes >4000 were also filtered out. Additionally, we removed a cluster with a high detection rate of the ribosome (>30%). In addition, genes that were detected in <10 cells were filtered out before further analyses. After quality control, data were normalized and scaled using the SCTransform function [102] , and a percentage of ribosomes was regressed out. We removed the batch effect across different individuals through the identification of anchors between individuals and passed these anchors to the IntegrateData function. For visualization, the dimensionality was further reduced using UMAP or t-Distributed Stochastic Neighbor Embedding. To cluster single cells based on their expression profiles, we used an unsupervised graph-based clustering algorithm, Louvain.

**Cell annotation**

The marker genes for each cluster were obtained using the FindAllMarkers function in Seurat package [101]. The MAST algorithm was used to calculate statistical significance. Genes that met the following criteria were considered signature genes: (1) adjusted p-value < 0.01 after Bonferroni correction by using all features in the dataset; (2) log fold-change of the average expression > 0.25; and (3) pct.1 > 0.25 (pct.1: the percentage of cells where the feature is detected in the first group); functional enrichment was performed on these genes to obtain cell type enriched pathways. The main cell types were defined using the SingleR package (https://bioconductor.org/packages/devel/bioc/htmL/SingleR.html). Then, we further

checked manually to confirm that reported cell type–specific expressed markers were specific for the corresponding clusters based on the following criteria: pct.1 > 0.6 and pct.2 < 0.4.

**Differential expression between groups**

For scRNAseq, DEGs were analyzed using the FindAllMarkers function in the Seurat package. The MAST algorithm was used to calculate statistical significance. Genes that met these criteria were considered DEGs: absolute log fold-change of the average expression ≥ 0.2 and pct > 0.1 (the percentage of cells where the feature is detected in either group). Functional enrichment was performed on these DEGs.

When calculating the difference in gene expression of bulk-seq, the number of reads that fall into each sample was obtained using htseq-count software [103] ; the data were standardized using the estimateSizeFactors function of the DESeq (2012) R package; and p-value and fold change value were calculated for difference comparison by using the nbinomTest function. Genes with a p-value < 0.05 and a fold difference >2 were defined as DEGs by bulk-seq.

**Functional enrichment analysis**

KEGG database and GO category database were used for the functional annotation of DEGs. The enrichment analysis of GO categories was performed by using the R clusterProfiler (v3.14.3) package, and the enrichment analysis of the pathways was performed on hypergeometric distribution by using the R phyper function. The GO categories with a false discovery rate < 0.05 were considered significantly enriched. Although pathways with p < 0.05 were regarded as enriched, only those GO categories or pathways containing ≥ 5 DEGs were kept for further analysis.

**Cell-Cell Communication**

To study the interactions between cells and to identify the mechanism by which the molecules communicate at a single-cell resolution, the R package CellChat (version 1.1.3) was applied [45]. Two types of interactions of the CellChatDB.mouse database were used: Secreted Signaling and Cell–Cell Contact. CellChat was used on each interaction separately. Using the aggregateNet function in CellChat, the aggregated cell–cell communication network was calculated, and the signaling from each cell

group was visualized. Outgoing or incoming signals of certain cell types were recognized using the function netAnalysis_signalingRole_heatmap.

**Cell differentiation trajectory inference**

To infer the differentiation of the trajectory of OPCs, we first used monocle (2.14.0) [104] to infer the pseudo time of each cell (method = "ICA", ordering_genes = marker genes).

**Immunofluorescence**

Mouse spinal cord tissue was fixed with 4% paraformaldehyde (Sinopharm Chemical Reagent Co. Ltd) overnight at 4 °C, embedded in Tissue Freezing Medium optimal cutting temperature compound (O.C.T) after dehydration in a gradient of 10%–30% sucrose solution. Then, 6-μm sections were prepared using a microtome (Leica, Wetzlar, Germany). The sections were rehydrated before immunofluorescence staining. For staining, the block was placed in 5% BSA supplemented with 1% Triton X-100 for 30 min at room temperature. Primary antibodies CD31 (AF3628, R&D Systems) and Col3a1 (sc-271249, Santa Cruz) were diluted in a 1:50 ratio with 0.01M PBS. The slides were placed in the cassette at 4 °C overnight. Then, they were diluted with a secondary antibody [Cy3-labeled Donkey Anti-Goat IgG(H+L); Alexa Fluor 488-labeled Goat Anti-Mouse IgG(H+L), Beyotime, Shanghai, China] in a 1:200 ratio with 0.01M PBS and incubated for 2 h at room temperature. They were washed three times with 0.01M PBS for 15 min each. Images were acquired with a fluorescence upright microscope (Zeiss Microscopy, Jena, Germany). The number of positive signals for each antibody in the spinal cord cross-section participated in the statistics.

**Competing interests**

The authors declare they have no competing interests.

**Funding**

This study was supported by the National Science Foundation of China (Grant No: 81701127 to X.L., Grant No: 32000841 to S.J.), the Municipal Health Commission of Nantong (Grant No: MA2020019 to Q.J.), the Science and Technology Bureau of

Nantong (Grant No: JC2020101 to Q.J.).

**Acknowledgements**

The authors thank Professor Yimin Hua from Nanjing Normal University for his valuable suggestions for this study; we also thank Lingfang Zhang from Suzhou Lingdian biotechnology Co. Ltd for his help with the bioinformatics analysis.

**Authors' Contributions**

J.S., L.X. and L.W. initiated and designed the study. J.S., J.Q., Q.Y., Q.J., R.Q., X.W., L.W., and L.X. performed the experiments and analyzed data. J.S., J.Q. and L.X. wrote the paper. All authors read and approved the manuscript.

**Reference**

[1] S. Lefebvre, L. Burglen, S. Reboullet, O. Clermont, P. Burlet, L. Viollet, B. Benichou, C. Cruaud, P. Millasseau, M. Zeviani, and et al., Identification and characterization of a spinal muscular atrophy-determining gene. Cell 80 (1995) 155-65.

[2] T.O. Crawford, and C.A. Pardo, The neurobiology of childhood spinal muscular atrophy. Neurobiol Dis 3 (1996) 97-110.

[3] C.L. Lorson, E. Hahnen, E.J. Androphy, and B. Wirth, A single nucleotide in the SMN gene regulates splicing and is responsible for spinal muscular atrophy. Proc Natl Acad Sci U S A 96 (1999) 6307-11.

[4] D.R. Corey, Nusinersen, an antisense oligonucleotide drug for spinal muscular atrophy. Nat Neurosci 20 (2017) 497-499.

[5] S. Dhillon, Risdiplam: First Approval. Drugs 80 (2020) 1853-1858.

[6] S.M. Hoy, Onasemnogene Abeparvovec: First Global Approval. Drugs 79 (2019) 1255-1262.

[7] B. Wirth, Spinal Muscular Atrophy: In the Challenge Lies a Solution. Trends Neurosci 44 (2021) 306-322.

[8] T.H. Coady, and C.L. Lorson, SMN in spinal muscular atrophy and snRNP biogenesis. Wiley Interdiscip Rev RNA 2 (2011) 546-64.

[9] W. Rossoll, S. Jablonka, C. Andreassi, A.K. Kroning, K. Karle, U.R. Monani, and M. Sendtner, Smn, the spinal muscular atrophy-determining gene product, modulates axon growth and localization of beta-actin mRNA in growth cones of motoneurons. J Cell Biol 163 (2003) 801-12.

[10] T.W. Prior, A.R. Krainer, Y. Hua, K.J. Swoboda, P.C. Snyder, S.J. Bridgeman, A.H. Burghes, and J.T. Kissel, A positive modifier of spinal muscular atrophy in the SMN2 gene. Am J Hum Genet 85 (2009) 408-13.

[11] X. Wu, S.H. Wang, J. Sun, A.R. Krainer, Y. Hua, and T.W. Prior, A-44G transition in SMN2 intron

6 protects patients with spinal muscular atrophy. Hum Mol Genet 26 (2017) 2768-2780.
[12] G.E. Oprea, S. Krober, M.L. McWhorter, W. Rossoll, S. Muller, M. Krawczak, G.J. Bassell, C.E. Beattie, and B. Wirth, Plastin 3 is a protective modifier of autosomal recessive spinal muscular atrophy. Science 320 (2008) 524-7.
[13] M. Riessland, A. Kaczmarek, S. Schneider, K.J. Swoboda, H. Lohr, C. Bradler, V. Grysko, M. Dimitriadi, S. Hosseinibarkooie, L. Torres-Benito, M. Peters, A. Upadhyay, N. Biglari, S. Krober, I. Holker, L. Garbes, C. Gilissen, A. Hoischen, G. Nurnberg, P. Nurnberg, M. Walter, F. Rigo, C.F. Bennett, M.J. Kye, A.C. Hart, M. Hammerschmidt, P. Kloppenburg, and B. Wirth, Neurocalcin Delta Suppression Protects against Spinal Muscular Atrophy in Humans and across Species by Restoring Impaired Endocytosis. Am J Hum Genet 100 (2017) 297-315.
[14] G.H. Park, Y. Maeno-Hikichi, T. Awano, L.T. Landmesser, and U.R. Monani, Reduced survival of motor neuron (SMN) protein in motor neuronal progenitors functions cell autonomously to cause spinal muscular atrophy in model mice expressing the human centromeric (SMN2) gene. J Neurosci 30 (2010) 12005-19.
[15] R.G. Gogliotti, K.A. Quinlan, C.B. Barlow, C.R. Heier, C.J. Heckman, and C.J. Didonato, Motor neuron rescue in spinal muscular atrophy mice demonstrates that sensory-motor defects are a consequence, not a cause, of motor neuron dysfunction. J Neurosci 32 (2012) 3818-29.
[16] J.V. McGivern, T.N. Patitucci, J.A. Nord, M.A. Barabas, C.L. Stucky, and A.D. Ebert, Spinal muscular atrophy astrocytes exhibit abnormal calcium regulation and reduced growth factor production. Glia 61 (2013) 1418-1428.
[17] S.L. Sison, T.N. Patitucci, E.R. Seminary, E. Villalon, C.L. Lorson, and A.D. Ebert, Astrocyte-produced miR-146a as a mediator of motor neuron loss in spinal muscular atrophy. Hum Mol Genet 26 (2017) 3409-3420.
[18] J.E. Martin, T.T. Nguyen, C. Grunseich, J.H. Nofziger, P.R. Lee, D. Fields, K.H. Fischbeck, and E. Foran, Decreased Motor Neuron Support by SMA Astrocytes due to Diminished MCP1 Secretion. J Neurosci 37 (2017) 5309-5318.
[19] C. Zhou, Z. Feng, and C.P. Ko, Defects in Motoneuron-Astrocyte Interactions in Spinal Muscular Atrophy. J Neurosci 36 (2016) 2543-53.
[20] H. Rindt, Z. Feng, C. Mazzasette, J.J. Glascock, D. Valdivia, N. Pyles, T.O. Crawford, K.J. Swoboda, T.N. Patitucci, A.D. Ebert, C.J. Sumner, C.P. Ko, and C.L. Lorson, Astrocytes influence the severity of spinal muscular atrophy. Hum Mol Genet 24 (2015) 4094-102.
[21] E. Somers, R.D. Lees, K. Hoban, J.N. Sleigh, H. Zhou, F. Muntoni, K. Talbot, T.H. Gillingwater, and S.H. Parson, Vascular Defects and Spinal Cord Hypoxia in Spinal Muscular Atrophy. Ann Neurol 79 (2016) 217-30.
[22] T.K. Doktor, Y. Hua, H.S. Andersen, S. Broner, Y.H. Liu, A. Wieckowska, M. Dembic, G.H. Bruun, A.R. Krainer, and B.S. Andresen, RNA-sequencing of a mouse-model of spinal muscular atrophy reveals tissue-wide changes in splicing of U12-dependent introns. Nucleic Acids Res 45 (2017) 395-416.
[23] Z. Zhang, A.M. Pinto, L. Wan, W. Wang, M.G. Berg, I. Oliva, L.N. Singh, C. Dengler, Z. Wei, and G. Dreyfuss, Dysregulation of synaptogenesis genes antecedes motor neuron pathology in spinal muscular atrophy. Proc Natl Acad Sci U S A 110 (2013) 19348-53.
[24] M. Maeda, A.W. Harris, B.F. Kingham, C.J. Lumpkin, L.M. Opdenaker, S.M. McCahan, W. Wang, and M.E. Butchbach, Transcriptome profiling of spinal muscular atrophy motor neurons

derived from mouse embryonic stem cells. PLoS One 9 (2014) e106818.
[25] S. Nichterwitz, J. Nijssen, H. Storvall, C. Schweingruber, L.H. Comley, I. Allodi, M.V. Lee, Q. Deng, R. Sandberg, and E. Hedlund, LCM-seq reveals unique transcriptional adaptation mechanisms of resistant neurons and identifies protective pathways in spinal muscular atrophy. Genome Res 30 (2020) 1083-1096.
[26] S. Corti, M. Nizzardo, C. Simone, M. Falcone, M. Nardini, D. Ronchi, C. Donadoni, S. Salani, G. Riboldi, F. Magri, G. Menozzi, C. Bonaglia, F. Rizzo, N. Bresolin, and G.P. Comi, Genetic correction of human induced pluripotent stem cells from patients with spinal muscular atrophy. Sci Transl Med 4 (2012) 165ra162.
[27] S.Y. Ng, B.S. Soh, N. Rodriguez-Muela, D.G. Hendrickson, F. Price, J.L. Rinn, and L.L. Rubin, Genome-wide RNA-Seq of Human Motor Neurons Implicates Selective ER Stress Activation in Spinal Muscular Atrophy. Cell Stem Cell 17 (2015) 569-84.
[28] F. Rizzo, M. Nizzardo, S. Vashisht, E. Molteni, V. Melzi, M. Taiana, S. Salani, P. Santonicola, E. Di Schiavi, M. Bucchia, A. Bordoni, I. Faravelli, N. Bresolin, G.P. Comi, U. Pozzoli, and S. Corti, Key role of SMN/SYNCRIP and RNA-Motif 7 in spinal muscular atrophy: RNA-Seq and motif analysis of human motor neurons. Brain 142 (2019) 276-294.
[29] J. Sun, Y. Song, Z. Chen, J. Qiu, S. Zhu, L. Wu, and L. Xing, Heterogeneity and Molecular Markers for CNS Glial Cells Revealed by Single-Cell Transcriptomics. Cell Mol Neurobiol (2021).
[30] A. Grubman, G. Chew, J.F. Ouyang, G. Sun, X.Y. Choo, C. McLean, R.K. Simmons, S. Buckberry, D.B. Vargas-Landin, D. Poppe, J. Pflueger, R. Lister, O.J.L. Rackham, E. Petretto, and J.M. Polo, A single-cell atlas of entorhinal cortex from individuals with Alzheimer's disease reveals cell-type-specific gene expression regulation. Nat Neurosci 22 (2019) 2087-2097.
[31] W. Liu, S. Venugopal, S. Majid, I.S. Ahn, G. Diamante, J. Hong, X. Yang, and S.H. Chandler, Single-cell RNA-seq analysis of the brainstem of mutant SOD1 mice reveals perturbed cell types and pathways of amyotrophic lateral sclerosis. Neurobiol Dis 141 (2020) 104877.
[32] S. Jakel, E. Agirre, A. Mendanha Falcao, D. van Bruggen, K.W. Lee, I. Knuesel, D. Malhotra, C. Ffrench-Constant, A. Williams, and G. Castelo-Branco, Altered human oligodendrocyte heterogeneity in multiple sclerosis. Nature 566 (2019) 543-547.
[33] Y. Nakata, T. Maeda, A. Kozuka, T. Hioka, Y. Mori, T. Ejiri, M. Kataoka, S. Hosoya, T. Ohnoshi, I. Kimura, and et al., [Idiopathic thrombocytopenic purpura in a patient with sarcoidosis]. Nihon Kyobu Shikkan Gakkai Zasshi 26 (1988) 700-6.
[34] S. Malaiya, M. Cortes-Gutierrez, B.R. Herb, S.R. Coffey, S.R.W. Legg, J.P. Cantle, C. Colantuoni, J.B. Carroll, and S.A. Ament, Single-Nucleus RNA-Seq Reveals Dysregulation of Striatal Cell Identity Due to Huntington's Disease Mutations. J Neurosci 41 (2021) 5534-5552.
[35] H.M. Hsieh-Li, J.G. Chang, Y.J. Jong, M.H. Wu, N.M. Wang, C.H. Tsai, and H. Li, A mouse model for spinal muscular atrophy. Nat Genet 24 (2000) 66-70.
[36] Y. Hua, K. Sahashi, F. Rigo, G. Hung, G. Horev, C.F. Bennett, and A.R. Krainer, Peripheral SMN restoration is essential for long-term rescue of a severe spinal muscular atrophy mouse model. Nature 478 (2011) 123-6.
[37] A.S. Reddy, D. O'Brien, N. Pisat, C.T. Weichselbaum, K. Sakers, M. Lisci, J.S. Dalal, and J.D. Dougherty, A Comprehensive Analysis of Cell Type-Specific Nuclear RNA From Neurons and Glia of the Brain. Biol Psychiatry 81 (2017) 252-264.
[38] A. Latremoliere, L. Cheng, M. DeLisle, C. Wu, S. Chew, E.B. Hutchinson, A. Sheridan, C.

Alexandre, F. Latremoliere, S.H. Sheu, S. Golidy, T. Omura, E.A. Huebner, Y. Fan, M.C. Whitman, E. Nguyen, C. Hermawan, C. Pierpaoli, M.A. Tischfield, C.J. Woolf, and E.C. Engle, Neuronal-Specific TUBB3 Is Not Required for Normal Neuronal Function but Is Essential for Timely Axon Regeneration. Cell Rep 24 (2018) 1865-1879 e9.

[39] Z. Feng, X. Ren, Y. Fang, Y. Yin, C. Huang, Y. Zhao, and Y. Wang, scTIM: seeking cell-type-indicative marker from single cell RNA-seq data by consensus optimization. Bioinformatics 36 (2020) 2474-2485.

[40] K.L. Fink, F. Lopez-Giraldez, I.J. Kim, S.M. Strittmatter, and W.B.J. Cafferty, Identification of Intrinsic Axon Growth Modulators for Intact CNS Neurons after Injury. Cell Rep 18 (2017) 2687-2701.

[41] Y. Zhang, K. Chen, S.A. Sloan, M.L. Bennett, A.R. Scholze, S. O'Keeffe, H.P. Phatnani, P. Guarnieri, C. Caneda, N. Ruderisch, S. Deng, S.A. Liddelow, C. Zhang, R. Daneman, T. Maniatis, B.A. Barres, and J.Q. Wu, An RNA-sequencing transcriptome and splicing database of glia, neurons, and vascular cells of the cerebral cortex. J Neurosci 34 (2014) 11929-47.

[42] Y. Yamazaki, N. Zhao, T.R. Caulfield, C.C. Liu, and G. Bu, Apolipoprotein E and Alzheimer disease: pathobiology and targeting strategies. Nat Rev Neurol 15 (2019) 501-518.

[43] L.M. Murray, A. Beauvais, S. Gibeault, N.L. Courtney, and R. Kothary, Transcriptional profiling of differentially vulnerable motor neurons at pre-symptomatic stage in the Smn (2b/-) mouse model of spinal muscular atrophy. Acta Neuropathol Commun 3 (2015) 55.

[44] D. Locatelli, M. Terao, M. Fratelli, A. Zanetti, M. Kurosaki, M. Lupi, M.M. Barzago, A. Uggetti, S. Capra, P. D'Errico, G.S. Battaglia, and E. Garattini, Human axonal survival of motor neuron (a-SMN) protein stimulates axon growth, cell motility, C-C motif ligand 2 (CCL2), and insulin-like growth factor-1 (IGF1) production. J Biol Chem 287 (2012) 25782-94.

[45] S. Jin, C.F. Guerrero-Juarez, L. Zhang, I. Chang, R. Ramos, C.H. Kuan, P. Myung, M.V. Plikus, and Q. Nie, Inference and analysis of cell-cell communication using CellChat. Nat Commun 12 (2021) 1088.

[46] K.K. Ling, M.Y. Lin, B. Zingg, Z. Feng, and C.P. Ko, Synaptic defects in the spinal and neuromuscular circuitry in a mouse model of spinal muscular atrophy. PLoS One 5 (2010) e15457.

[47] M.F. Lanfranco, C.A. Ng, and G.W. Rebeck, ApoE Lipidation as a Therapeutic Target in Alzheimer's Disease. Int J Mol Sci 21 (2020).

[48] A. Cheng, W. Jia, I. Kawahata, and K. Fukunaga, A novel fatty acid-binding protein 5 and 7 inhibitor ameliorates oligodendrocyte injury in multiple sclerosis mouse models. EBioMedicine 72 (2021) 103582.

[49] S. Foerster, A. Guzman de la Fuente, Y. Kagawa, T. Bartels, Y. Owada, and R.J.M. Franklin, The fatty acid binding protein FABP7 is required for optimal oligodendrocyte differentiation during myelination but not during remyelination. Glia 68 (2020) 1410-1420.

[50] G. Helfer, and Q.F. Wu, Chemerin: a multifaceted adipokine involved in metabolic disorders. J Endocrinol 238 (2018) R79-R94.

[51] C.J.J. Yeo, and B.T. Darras, Overturning the Paradigm of Spinal Muscular Atrophy as Just a Motor Neuron Disease. Pediatr Neurol 109 (2020) 12-19.

[52] Y. Hua, Y.H. Liu, K. Sahashi, F. Rigo, C.F. Bennett, and A.R. Krainer, Motor neuron cell-nonautonomous rescue of spinal muscular atrophy phenotypes in mild and severe transgenic mouse models. Genes Dev 29 (2015) 288-97.

[53] Z. Zhang, F. Lotti, K. Dittmar, I. Younis, L. Wan, M. Kasim, and G. Dreyfuss, SMN deficiency causes tissue-specific perturbations in the repertoire of snRNAs and widespread defects in splicing. Cell 133 (2008) 585-600.

[54] D. Baumer, S. Lee, G. Nicholson, J.L. Davies, N.J. Parkinson, L.M. Murray, T.H. Gillingwater, O. Ansorge, K.E. Davies, and K. Talbot, Alternative splicing events are a late feature of pathology in a mouse model of spinal muscular atrophy. PLoS Genet 5 (2009) e1000773.

[55] L.M. Murray, S. Lee, D. Baumer, S.H. Parson, K. Talbot, and T.H. Gillingwater, Pre-symptomatic development of lower motor neuron connectivity in a mouse model of severe spinal muscular atrophy. Hum Mol Genet 19 (2010) 420-33.

[56] J.F. Staropoli, H. Li, S.J. Chun, N. Allaire, P. Cullen, A. Thai, C.M. Fleet, Y. Hua, C.F. Bennett, A.R. Krainer, D. Kerr, A. McCampbell, F. Rigo, and J.P. Carulli, Rescue of gene-expression changes in an induced mouse model of spinal muscular atrophy by an antisense oligonucleotide that promotes inclusion of SMN2 exon 7. Genomics 105 (2015) 220-8.

[57] S. Balabanian, N.H. Gendron, and A.E. MacKenzie, Histologic and transcriptional assessment of a mild SMA model. Neurol Res 29 (2007) 413-24.

[58] Q. Huo, M. Kayikci, P. Odermatt, K. Meyer, O. Michels, S. Saxena, J. Ule, and D. Schumperli, Splicing changes in SMA mouse motoneurons and SMN-depleted neuroblastoma cells: evidence for involvement of splicing regulatory proteins. RNA Biol 11 (2014) 1430-46.

[59] F. Richter, B.H. Meurers, C. Zhu, V.P. Medvedeva, and M.F. Chesselet, Neurons express hemoglobin alpha- and beta-chains in rat and human brains. J Comp Neurol 515 (2009) 538-47.

[60] D.W. Schelshorn, A. Schneider, W. Kuschinsky, D. Weber, C. Kruger, T. Dittgen, H.F. Burgers, F. Sabouri, N. Gassler, A. Bach, and M.H. Maurer, Expression of hemoglobin in rodent neurons. J Cereb Blood Flow Metab 29 (2009) 585-95.

[61] R.C. Shah, J.A. Schneider, S. Leurgans, and D.A. Bennett, Association of lower hemoglobin level and neuropathology in community-dwelling older persons. J Alzheimers Dis 32 (2012) 579-86.

[62] N. Brown, K. Alkhayer, R. Clements, N. Singhal, R. Gregory, S. Azzam, S. Li, E. Freeman, and J. McDonough, Neuronal Hemoglobin Expression and Its Relevance to Multiple Sclerosis Neuropathology. J Mol Neurosci 59 (2016) 1-17.

[63] L. Bianchi, M. Sframeli, L. Vantaggiato, G.L. Vita, A. Ciranni, F. Polito, R. Oteri, E. Gitto, F. Di Giuseppe, S. Angelucci, A. Versaci, S. Messina, G. Vita, L. Bini, and M. Aguennouz, Nusinersen Modulates Proteomics Profiles of Cerebrospinal Fluid in Spinal Muscular Atrophy Type 1 Patients. Int J Mol Sci 22 (2021).

[64] M.O. Deguise, L. Chehade, and R. Kothary, Metabolic Dysfunction in Spinal Muscular Atrophy. Int J Mol Sci 22 (2021).

[65] N.J. Allen, and D.A. Lyons, Glia as architects of central nervous system formation and function. Science 362 (2018) 181-185.

[66] E. Abati, G. Citterio, N. Bresolin, G.P. Comi, and S. Corti, Glial cells involvement in spinal muscular atrophy: Could SMA be a neuroinflammatory disease? Neurobiol Dis 140 (2020) 104870.

[67] C. Soubrouillard, J.F. Pellissier, H. Lepidi, J. Mancini, G. Rougon, and D. Figarella-Branger, Expression of developmentally regulated cytoskeleton and cell surface proteins in childhood spinal muscular atrophies. J Neurol Sci 133 (1995) 155-63.

[68] M. Murdocca, S.A. Ciafre, P. Spitalieri, R.V. Talarico, M. Sanchez, G. Novelli, and F. Sangiuolo, SMA Human iPSC-Derived Motor Neurons Show Perturbed Differentiation and Reduced miR-335-5p Expression. Int J Mol Sci 17 (2016).

[69] S. Hauser, S. Schuster, E. Heuten, P. Hoflinger, J. Admard, Y. Schelling, A. Velic, B. Macek, S. Ossowski, and L. Schols, Comparative Transcriptional Profiling of Motor Neuron Disorder-Associated Genes in Various Human Cell Culture Models. Front Cell Dev Biol 8 (2020) 544043.

[70] J.A. Blum, S. Klemm, J.L. Shadrach, K.A. Guttenplan, L. Nakayama, A. Kathiria, P.T. Hoang, O. Gautier, J.A. Kaltschmidt, W.J. Greenleaf, and A.D. Gitler, Single-cell transcriptomic analysis of the adult mouse spinal cord reveals molecular diversity of autonomic and skeletal motor neurons. Nat Neurosci 24 (2021) 572-583.

[71] K.K. Ling, R.M. Gibbs, Z. Feng, and C.P. Ko, Severe neuromuscular denervation of clinically relevant muscles in a mouse model of spinal muscular atrophy. Hum Mol Genet 21 (2012) 185-95.

[72] T.L. Martinez, L. Kong, X. Wang, M.A. Osborne, M.E. Crowder, J.P. Van Meerbeke, X. Xu, C. Davis, J. Wooley, D.J. Goldhamer, C.M. Lutz, M.M. Rich, and C.J. Sumner, Survival motor neuron protein in motor neurons determines synaptic integrity in spinal muscular atrophy. J Neurosci 32 (2012) 8703-15.

[73] S. Hickman, S. Izzy, P. Sen, L. Morsett, and J. El Khoury, Microglia in neurodegeneration. Nat Neurosci 21 (2018) 1359-1369.

[74] G. Khayrullina, Z.A. Alipio-Gloria, M.O. Deguise, S. Gagnon, L. Chehade, M. Stinson, N. Belous, E.M. Bergman, F.W. Lischka, J. Rotty, C.L. Dalgard, R. Kothary, K.A. Johnson, and B.G. Burnett, Survival motor neuron protein deficiency alters microglia reactivity. Glia 70 (2022) 1337-1358.

[75] O. Tarabal, V. Caraballo-Miralles, A. Cardona-Rossinyol, F.J. Correa, G. Olmos, J. Llado, J.E. Esquerda, and J. Caldero, Mechanisms involved in spinal cord central synapse loss in a mouse model of spinal muscular atrophy. J Neuropathol Exp Neurol 73 (2014) 519-35.

[76] A. Vukojicic, N. Delestree, E.V. Fletcher, J.G. Pagiazitis, S. Sankaranarayanan, T.A. Yednock, B.A. Barres, and G.Z. Mentis, The Classical Complement Pathway Mediates Microglia-Dependent Remodeling of Spinal Motor Circuits during Development and in SMA. Cell Rep 29 (2019) 3087-3100 e7.

[77] M.V. Sofroniew, Astrocyte Reactivity: Subtypes, States, and Functions in CNS Innate Immunity. Trends Immunol 41 (2020) 758-770.

[78] S.A. Liddelow, K.A. Guttenplan, L.E. Clarke, F.C. Bennett, C.J. Bohlen, L. Schirmer, M.L. Bennett, A.E. Munch, W.S. Chung, T.C. Peterson, D.K. Wilton, A. Frouin, B.A. Napier, N. Panicker, M. Kumar, M.S. Buckwalter, D.H. Rowitch, V.L. Dawson, T.M. Dawson, B. Stevens, and B.A. Barres, Neurotoxic reactive astrocytes are induced by activated microglia. Nature 541 (2017) 481-487.

[79] J.L. Zamanian, L. Xu, L.C. Foo, N. Nouri, L. Zhou, R.G. Giffard, and B.A. Barres, Genomic analysis of reactive astrogliosis. J Neurosci 32 (2012) 6391-410.

[80] L.E. Clarke, S.A. Liddelow, C. Chakraborty, A.E. Munch, M. Heiman, and B.A. Barres, Normal aging induces A1-like astrocyte reactivity. Proc Natl Acad Sci U S A 115 (2018) E1896-E1905.

[81] C. Stadelmann, S. Timmler, A. Barrantes-Freer, and M. Simons, Myelin in the Central Nervous

System: Structure, Function, and Pathology. Physiol Rev 99 (2019) 1381-1431.
[82] R.W. O'Meara, S.E. Cummings, Y. De Repentigny, E. McFall, J.P. Michalski, M.O. Deguise, S. Gibeault, and R. Kothary, Oligodendrocyte development and CNS myelination are unaffected in a mouse model of severe spinal muscular atrophy. Hum Mol Genet 26 (2017) 282-292.
[83] K. Ohuchi, M. Funato, S. Ando, S. Inagaki, A. Sato, C. Kawase, J. Seki, S. Nakamura, M. Shimazawa, H. Kaneko, and H. Hara, Impairment of oligodendrocyte lineages in spinal muscular atrophy model systems. Neuroreport 30 (2019) 350-357.
[84] M.D. Sweeney, K. Kisler, A. Montagne, A.W. Toga, and B.V. Zlokovic, The role of brain vasculature in neurodegenerative disorders. Nat Neurosci 21 (2018) 1318-1331.
[85] C.E. Dorrier, H.E. Jones, L. Pintaric, J.A. Siegenthaler, and R. Daneman, Emerging roles for CNS fibroblasts in health, injury and disease. Nat Rev Neurosci 23 (2022) 23-34.
[86] A. Araujo, M. Araujo, and K.J. Swoboda, Vascular perfusion abnormalities in infants with spinal muscular atrophy. J Pediatr 155 (2009) 292-4.
[87] S. Rudnik-Schoneborn, S. Vogelgesang, S. Armbrust, L. Graul-Neumann, C. Fusch, and K. Zerres, Digital necroses and vascular thrombosis in severe spinal muscular atrophy. Muscle Nerve 42 (2010) 144-7.
[88] E. Somers, Z. Stencel, T.M. Wishart, T.H. Gillingwater, and S.H. Parson, Density, calibre and ramification of muscle capillaries are altered in a mouse model of severe spinal muscular atrophy. Neuromuscul Disord 22 (2012) 435-42.
[89] J.M. Ross, C. Kim, D. Allen, E.E. Crouch, K. Narsinh, D.L. Cooke, A.A. Abla, T.J. Nowakowski, and E.A. Winkler, The Expanding Cell Diversity of the Brain Vasculature. Front Physiol 11 (2020) 600767.
[90] M. Vanlandewijck, L. He, M.A. Mae, J. Andrae, K. Ando, F. Del Gaudio, K. Nahar, T. Lebouvier, B. Lavina, L. Gouveia, Y. Sun, E. Raschperger, M. Rasanen, Y. Zarb, N. Mochizuki, A. Keller, U. Lendahl, and C. Betsholtz, A molecular atlas of cell types and zonation in the brain vasculature. Nature 554 (2018) 475-480.
[91] A. Zeisel, H. Hochgerner, P. Lonnerberg, A. Johnsson, F. Memic, J. van der Zwan, M. Haring, E. Braun, L.E. Borm, G. La Manno, S. Codeluppi, A. Furlan, K. Lee, N. Skene, K.D. Harris, J. Hjerling-Leffler, E. Arenas, P. Ernfors, U. Marklund, and S. Linnarsson, Molecular Architecture of the Mouse Nervous System. Cell 174 (2018) 999-1014 e22.
[92] C.E. Dorrier, D. Aran, E.A. Haenelt, R.N. Sheehy, K.K. Hoi, L. Pintaric, Y. Chen, C.O. Lizama, K.M. Cautivo, G.A. Weiner, B. Popko, S.P.J. Fancy, T.D. Arnold, and R. Daneman, CNS fibroblasts form a fibrotic scar in response to immune cell infiltration. Nat Neurosci 24 (2021) 234-244.
[93] X.M. Cao, S.L. Li, Y.Q. Cao, Y.H. Lv, Y.X. Wang, B. Yu, and C. Yao, A comparative analysis of differentially expressed genes in rostral and caudal regions after spinal cord injury in rats. Neural Regen Res 17 (2022) 2267-2271.
[94] A.C. Yang, R.T. Vest, F. Kern, D.P. Lee, M. Agam, C.A. Maat, P.M. Losada, M.B. Chen, N. Schaum, N. Khoury, A. Toland, K. Calcuttawala, H. Shin, R. Palovics, A. Shin, E.Y. Wang, J. Luo, D. Gate, W.J. Schulz-Schaeffer, P. Chu, J.A. Siegenthaler, M.W. McNerney, A. Keller, and T. Wyss-Coray, A human brain vascular atlas reveals diverse mediators of Alzheimer's risk. Nature 603 (2022) 885-892.
[95] A. Manberg, N. Skene, F. Sanders, M. Trusohamn, J. Remnestal, A. Szczepinska, I.S. Aksoylu, P.

Lonnerberg, L. Ebarasi, S. Wouters, M. Lehmann, J. Olofsson, I. von Gohren Antequera, A. Domaniku, M. De Schaepdryver, J. De Vocht, K. Poesen, M. Uhlen, J. Anink, C. Mijnsbergen, H. Vergunst-Bosch, A. Hubers, U. Klappe, E. Rodriguez-Vieitez, J.D. Gilthorpe, E. Hedlund, R.A. Harris, E. Aronica, P. Van Damme, A. Ludolph, J. Veldink, C. Ingre, P. Nilsson, and S.A. Lewandowski, Altered perivascular fibroblast activity precedes ALS disease onset. Nat Med 27 (2021) 640-646.

[96] N. Miller, H. Shi, A.S. Zelikovich, and Y.C. Ma, Motor neuron mitochondrial dysfunction in spinal muscular atrophy. Hum Mol Genet 25 (2016) 3395-3406.

[97] B. Wan, P. Feng, Z. Guan, L. Sheng, Z. Liu, and Y. Hua, A severe mouse model of spinal muscular atrophy develops early systemic inflammation. Hum Mol Genet 27 (2018) 4061-4076.

[98] D.J. Graber, and B.T. Harris, Purification and culture of spinal motor neurons from rat embryos. Cold Spring Harb Protoc 2013 (2013) 319-26.

[99] D. Kim, B. Langmead, and S.L. Salzberg, HISAT: a fast spliced aligner with low memory requirements. Nat Methods 12 (2015) 357-60.

[100] C. Trapnell, B.A. Williams, G. Pertea, A. Mortazavi, G. Kwan, M.J. van Baren, S.L. Salzberg, B.J. Wold, and L. Pachter, Transcript assembly and quantification by RNA-Seq reveals unannotated transcripts and isoform switching during cell differentiation. Nat Biotechnol 28 (2010) 511-5.

[101] T. Stuart, A. Butler, P. Hoffman, C. Hafemeister, E. Papalexi, W.M. Mauck, 3rd, Y. Hao, M. Stoeckius, P. Smibert, and R. Satija, Comprehensive Integration of Single-Cell Data. Cell 177 (2019) 1888-1902 e21.

[102] C. Hafemeister, and R. Satija, Normalization and variance stabilization of single-cell RNA-seq data using regularized negative binomial regression. Genome Biol 20 (2019) 296.

[103] S. Anders, P.T. Pyl, and W. Huber, HTSeq--a Python framework to work with high-throughput sequencing data. Bioinformatics 31 (2015) 166-9.

[104] X. Qiu, Q. Mao, Y. Tang, L. Wang, R. Chawla, H.A. Pliner, and C. Trapnell, Reversed graph embedding resolves complex single-cell trajectories. Nat Methods 14 (2017) 979-982.

## Figure legends

Figure 1. Cell type identification.

(A) UMAP visualization showing the cluster of cell type from scRNAseq. (B) The heatmap shows the average expression of marker genes for each cell type. The darker the yellow, the higher the expression level. (C) The proportion of each cell type to the total number of cells. (D) UMAP visualization showing the distribution of SMA and control cells. (E) Proportion of cells from SMA or control samples in each cell type.

Sup 1. Cell type identification.

(A) The average expression of each marker gene in different cell types; the darker the red, the higher the expression. (B) UMAP visualization shows the expression of marker

genes in different cell types; the darker the red, the higher the expression.

Figure 2. Analysis of DEGs and functions of scRNAseq and bulk-seq.

(A) The number of DEGs in different cell types in scRNAseq. (B) Number of DEGs in bulk-seq. (C) A volcano plot showing DEGs in neurons. (D) Volcano plot showing DEGs of the vasculature. The x-axis represents logFC, and the y-axis represents log10 p-value. (E) GO analysis of DEGs in several cell types; the X-axis represents log10 p-value. Four cell types are not shown in the figure. The results of Schwann cells, OPCs, and COPs are similar to that of OLs, and the p-value of ependymal cells is $>10^{-5}$. (F) An overlap gene analysis of cell-type-specific DEGs and bulk-seq DEGs; the y-axis represents the number of genes, and the x-axis represents the number of cell types; for example, the column with the column head "3" represents the number of overlapping DEGs of the bulk-seq and two cell types. (G) We analyzed whether the change trends of cell-type-specific DEGs in scRNAseq and DEGs of bulk-seq are the same; blue indicates the same trend, and both are downregulated, red indicates the same trend, and both are upregulated, and gray indicates opposite trends.

Sup 2. Analysis of DEGs and functions of scRNAseq and bulk-seq.

(A) The number of genes detected through scRNAseq in each cell type. (B) The expression of the Xist gene is mainly related to gender, and its FPKM value in the bulk-seq of female samples is much larger than that in the bulk-seq of male samples. (C) The cell-type–specific DEGs and bulk-seq DEGs were intersected, and the heatmap shows the expression changes in the intersected genes in different cell types and bulk-seq. (D) Violin plots of Hba-a1, Hbb-bt, and Tmsb10 expression in different cell types and bulk-seq. (E) KEGG pathway analysis of cell-type–specific DEGs and DEGs by bulk-seq; red indicates upregulated pathways, and blue indicates downregulated pathways.

Figure 3. Cell–cell communication is reduced in the spinal cord of SMA mice.

(A) Overall number and strength of cell–cell communication based on CCI. (B, C) Differences in the (B) number and (C) strength of CCI communication of various cell

types between SMA mice and control mice. The blue line indicates decreased communication, and the red line indicates increased communication. The thicker the line, the greater the difference. (D) Overall number and strength of cell–cell communication based on SSI. (E, F) Differences in the number (E) and strength (F) of SSI communication of various cell types between SMA and control mice. The blue line indicates decreased communication, and the red line indicates increased communication. The thicker the line, the greater the difference. (G, H) Receptor–ligand pairs that differ significantly between SMA and controls based on SSI (G) and CCI (H).

Figure 4. Identified cell subtypes and DEGs of cell subtypes.
(A–E) Analysis of cell subtypes of (A) astrocytes, (B) ependymal cells, (C) microglia, (D) OL lineages, and (E) vasculature by UMAP. (F) Number of DEGs for each cell subtype.

Sup 3. Identify cell subtypes and DEGs of cell subtypes.
The average expression of markers of each cell subtype of SMA, the darker the red, the higher the expression; A, C, E, G, and I represent astrocytes, ependymal cells, microglia, OL lineages, and vasculature, respectively. KEGG analysis of marker genes for each cell subtype; B, D, F, H, and J represent astrocytes, ependymal cells, microglia, OL lineages, and vasculature, respectively.

Figure 5. Altered gene expression of several glial cell subtypes in the SMA spinal cord.
(A) Volcano plot of DEGs in MG-5 subpopulations. (B) BP analysis of DEGs in MG-5 subtypes; the top 5 most significant terms are shown: red indicates upregulated terms, and blue indicates downregulated terms. (C) Volcano plot of DEGs in OL-5 subpopulations. (D) Signature DEGs expression of OL-5. (E, F) BP and cellular component analysis of DEGs in OL-5; the top 5 most significant terms are shown. (G) Pseudo time analysis of individual cell subtypes in OL lineages. The x-axis represents the cell subtype. The value of the y-axis represents the order of time. The smaller the value, the stronger the characteristics of the progenitor cells. The larger the value, the

more mature (later) the cell is. p-values were calculated through the t-test, ns: $p > 0.05$, *: $p < 0.05$, ***: $p < 0.001$, ****: $p < 0.0001$.

Sup 4. Altered gene expression of several glial cell subtypes in the SMA spinal cord. (A–C) Comparison of cell numbers of various subtypes of astrocyte, microglia, and OL lineage in SMA and control mice. (D) UMAP visualization showing the expression of Apoe, and Fabp7 in all cells. (E) The position of each subtype of OL lineage on the pseudo time trajectory maturing from right to left. (F, G) Pseudo time trajectory of OL lineage in SMA (right) and control (left) mice, and the location of OL-5 on the pseudo time trajectory.

Fig. 6. A subpopulation of vascular fibroblasts is drastically reduced in SMA spinal cord. (A) UMAP visualization showing the subtypes of vasculature in control and SMA mice. Vas-2 is marked by red circles. (B) Comparison of the cell numbers of various subtypes in the vasculature of SMA and control mice. (C) Violin plots showing the expression of fibroblast marker genes in vasculature subtypes. (D, E) UMAP visualization showing the expression of Col3a1 and Rarres2 in the vasculature of SMA and control mice. (F) Expression analysis of the top 13 most significant DEGs in two fibroblast subtypes, Vas-2 and Vas-3. (G) Immunofluorescence staining of spinal cord transections in SMA and control mice. Here, 4′,6-diamidino-2-phenylindole (DAPI)-labeled nuclei are indicated in blue, Col3a1-labeled fibroblasts are indicated in green, and CD31-labeled vascular endothelial cells are indicated in red. Bar = 50 μm. (H) Statistical results of staining for CD31 and Col3a1. The P-value is calculated by Student's t-test, n = 3, bars represent the mean with SEM. (I) Expression analysis of protein synthesis (translation) and energy metabolism (ATP metabolic process) pathways of various cell types in SMA and control mice. p-values were calculated through the t-test, ns: $p > 0.05$, *: $p < 0.05$, **: $p < 0.01$, ***: $p < 0.001$, ****: $p < 0.0001$.

Sup 5. Expression analysis of protein synthesis and energy metabolism-related

pathways in SMA and control mice. p-values were calculated by t-test.

Sup File 1. Gene list for bulk-seq and cell-type–specific DEGs. SMA vs. control.

Sup File 2. DEG lists for all cell subtypes. SMA vs. control.

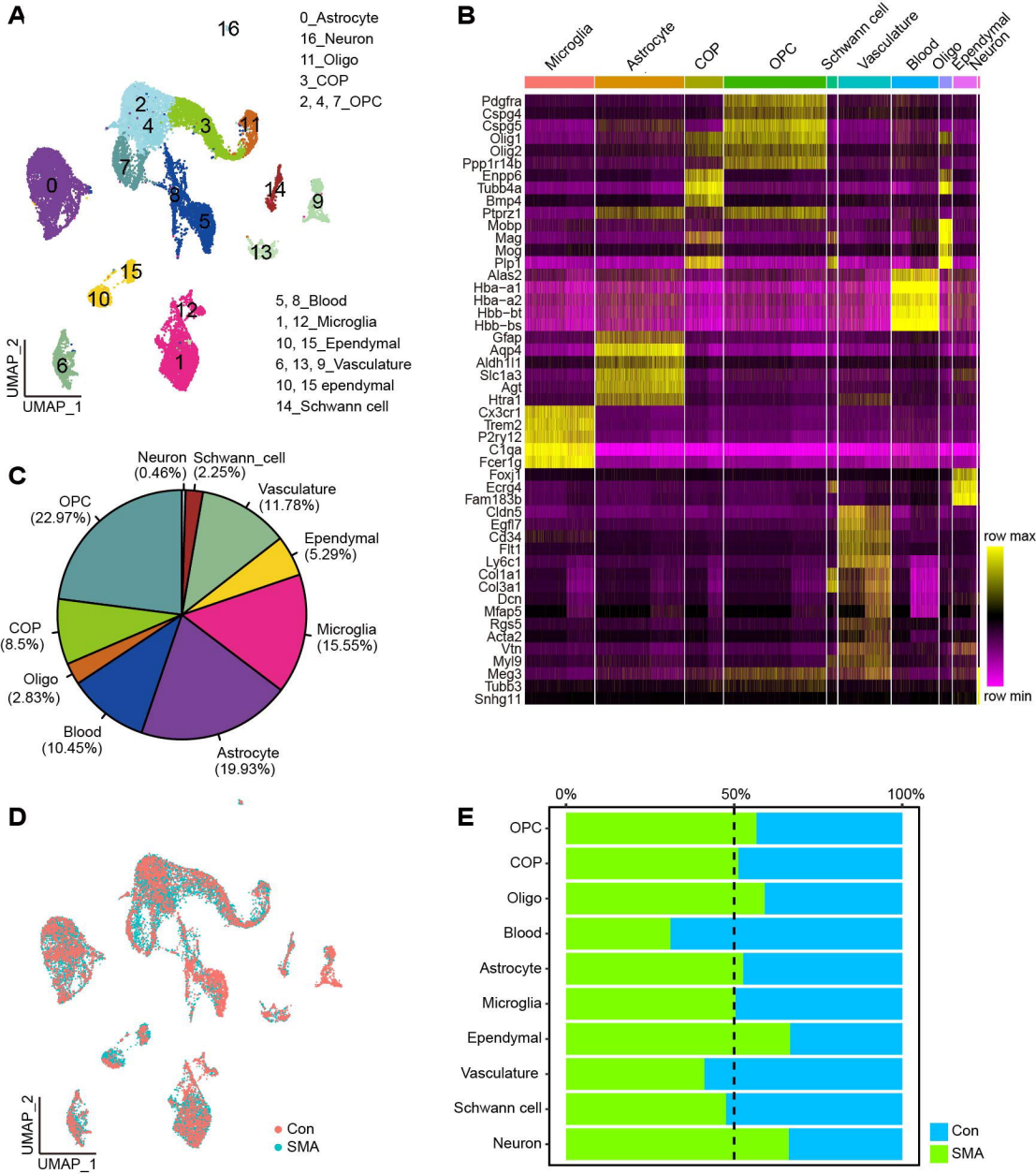
A
0_Astrocyte
16_Neuron
11_Oligo
3_COP
2, 4, 7_OPC
5, 8_Blood
1, 12_Microglia
10, 15_Ependymal
6, 13, 9_Vasculature
10, 15 ependymal
14_Schwann cell
UMAP_2
UMAP_1
B
Microglia
Astrocyte
COP
OPC
Schwann cell
Vasculature
Blood
Oligo
Ependymal
Neuron
Pdgfra
Cspg4
Cspg5
Olig1
Olig2
Ppp1r14b
Enpp6
Tubb4a
Bmp4
Ptprz1
Mobp
Mag
Mog
Plp1
Alas2
Hba-a1
Hba-a2
Hbb-bt
Hbb-bs
Gfap
Aqp4
Aldh1l1
Slc1a3
Agt
Htra1
Cx3cr1
Trem2
P2ry12
C1qa
Fcer1g
Foxj1
Ecrg4
Fam183b
Cldn5
Egfl7
Cd34
Flt1
Ly6c1
Col1a1
Col3a1
Dcn
Mfap5
Rgs5
Acta2
Vtn
Myl9
Meg3
Tubb3
Snhg11
row max
row min
C
Neuron (0.46%)
Schwann_cell (2.25%)
Vasculature (11.78%)
Ependymal (5.29%)
Microglia (15.55%)
Astrocyte (19.93%)
Blood (10.45%)
Oligo (2.83%)
COP (8.5%)
OPC (22.97%)
D
Con
SMA
UMAP_2
UMAP_1
E
0%
50%
100%
OPC
COP
Oligo
Blood
Astrocyte
Microglia
Ependymal
Vasculature
Schwann cell
Neuron
Con
SMA

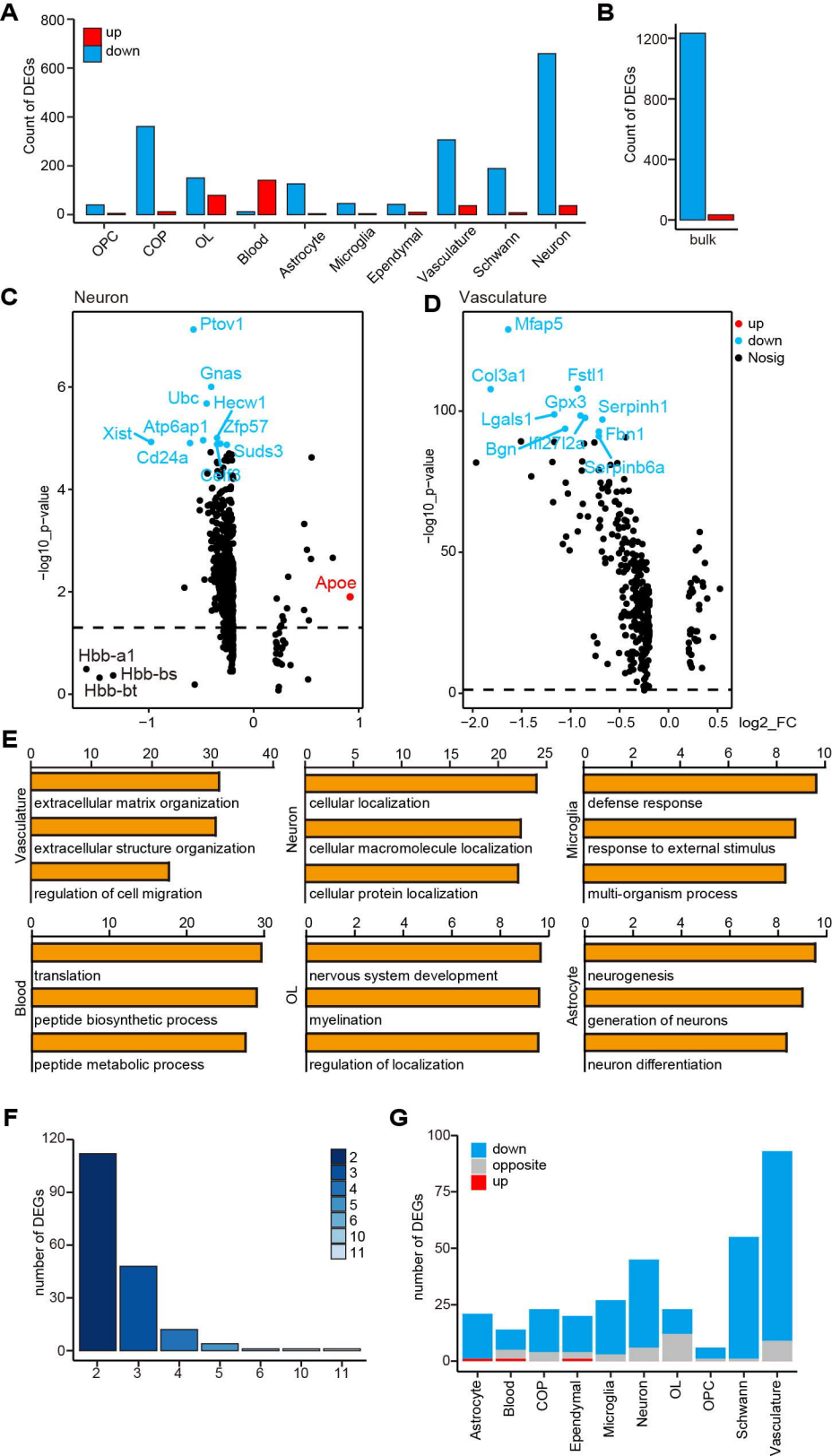
A
up
down
Count of DEGs
OPC
COP
OL
Blood
Astrocyte
Microglia
Ependymal
Vasculature
Schwann
Neuron
B
Count of DEGs
bulk
C
Neuron
Ptov1
Gnas
Ubc
Hecw1
Xist
Atp6ap1
Zfp57
Cd24a
Suds3
Apoe
Hbb-a1
Hbb-bs
Hbb-bt
−log10_p−value
D
Vasculature
Mfap5
Col3a1
Fstl1
Gpx3
Serpinh1
Lgals1
Fbn1
Bgn
Serpinb6a
up
down
Nosig
−log10_p−value
log2_FC
E
Vasculature
extracellular matrix organization
extracellular structure organization
regulation of cell migration
Neuron
cellular localization
cellular macromolecule localization
cellular protein localization
Microglia
defense response
response to external stimulus
multi-organism process
Blood
translation
peptide biosynthetic process
peptide metabolic process
OL
nervous system development
myelination
regulation of localization
Astrocyte
neurogenesis
generation of neurons
neuron differentiation
F
number of DEGs
2
3
4
5
6
10
11
G
down
opposite
up
number of DEGs
Astrocyte
Blood
COP
Ependymal
Microglia
Neuron
OL
OPC
Schwann
Vasculature

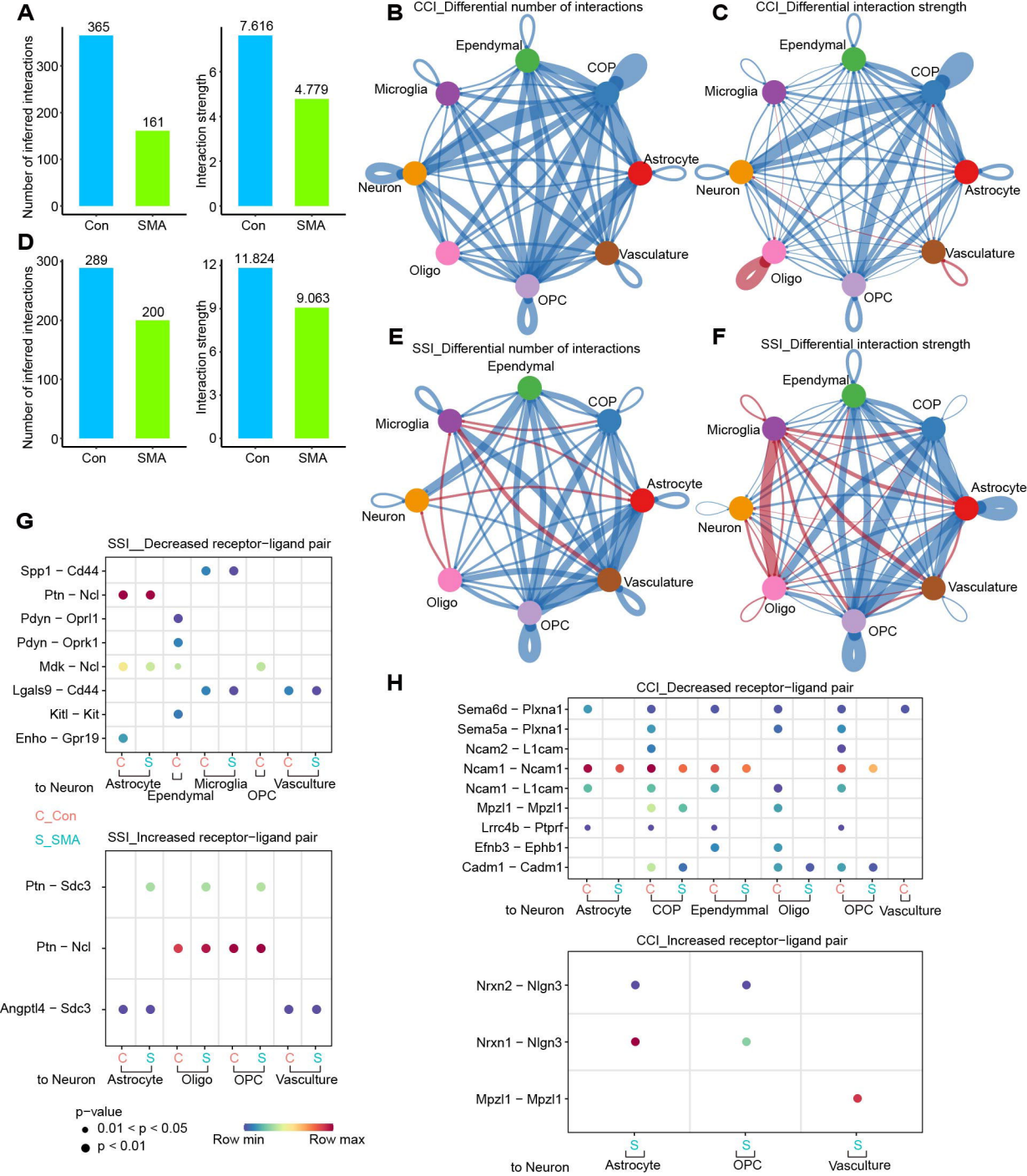
A
Number of inferred interactions
365
161
Con
SMA
Interaction strength
7.616
4.779
B
CCI_Differential number of interactions
Ependymal
COP
Microglia
Astrocyte
Neuron
Vasculature
Oligo
OPC
C
CCI_Differential interaction strength
D
289
200
11.824
9.063
E
SSI_Differential number of interactions
F
SSI_Differential interaction strength
G
SSI__Decreased receptor−ligand pair
Spp1 − Cd44
Ptn − Ncl
Pdyn − Oprl1
Pdyn − Oprk1
Mdk − Ncl
Lgals9 − Cd44
Kitl − Kit
Enho − Gpr19
to Neuron
Astrocyte
Ependymal
Microglia
OPC
Vasculture
C_Con
S_SMA
SSI_Increased receptor−ligand pair
Ptn − Sdc3
Ptn − Ncl
Angptl4 − Sdc3
Oligo
p−value
0.01 < p < 0.05
p < 0.01
Row min
Row max
H
CCI_Decreased receptor−ligand pair
Sema6d − Plxna1
Sema5a − Plxna1
Ncam2 − L1cam
Ncam1 − Ncam1
Ncam1 − L1cam
Mpzl1 − Mpzl1
Lrrc4b − Ptprf
Efnb3 − Ephb1
Cadm1 − Cadm1
COP
Ependymmal
Vasculture
CCI_Increased receptor−ligand pair
Nrxn2 − Nlgn3
Nrxn1 − Nlgn3
Mpzl1 − Mpzl1

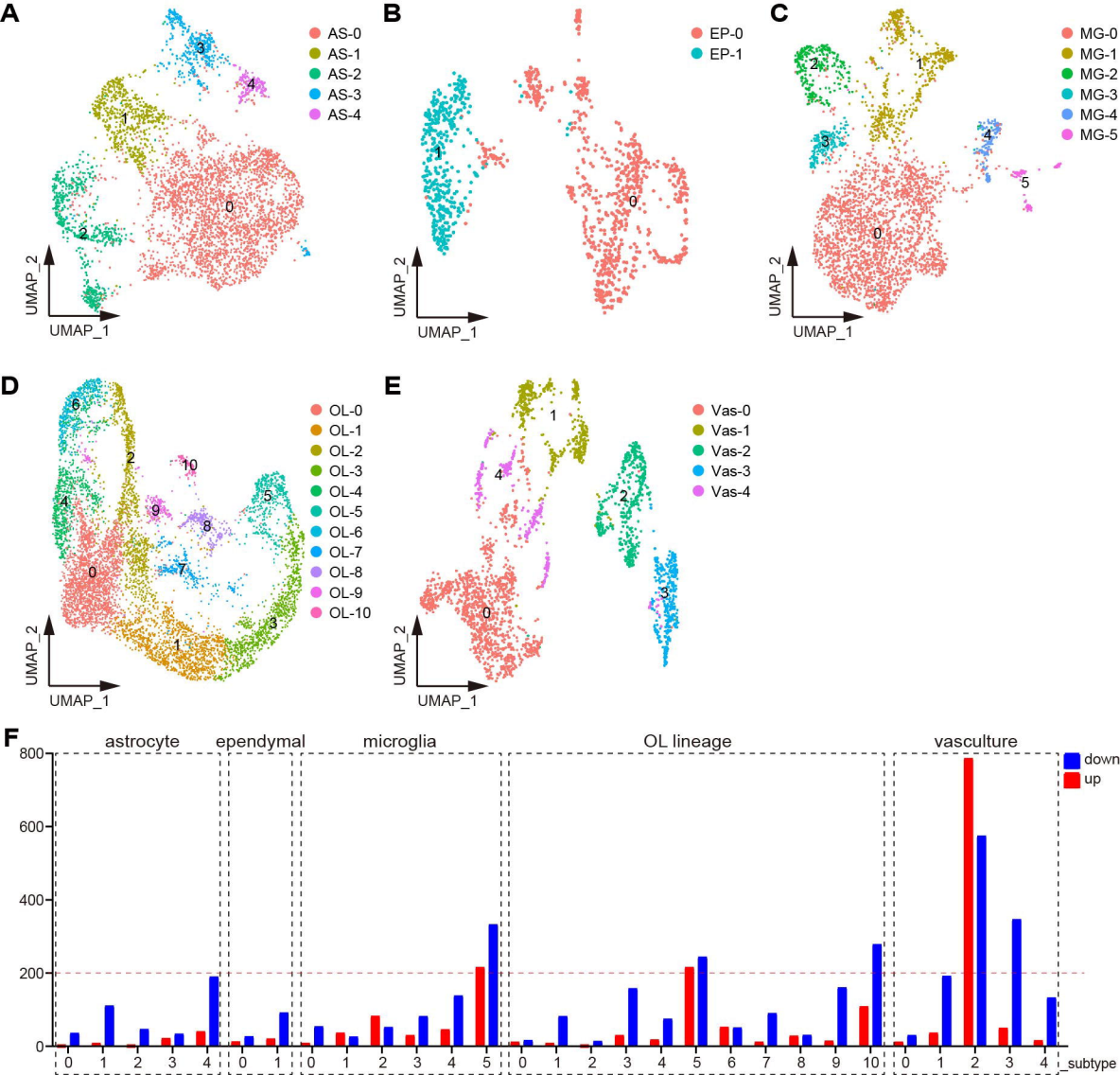
A
AS-0
AS-1
AS-2
AS-3
AS-4
UMAP_2
UMAP_1
B
EP-0
EP-1
UMAP_2
UMAP_1
C
MG-0
MG-1
MG-2
MG-3
MG-4
MG-5
UMAP_2
UMAP_1
D
OL-0
OL-1
OL-2
OL-3
OL-4
OL-5
OL-6
OL-7
OL-8
OL-9
OL-10
UMAP_2
UMAP_1
E
Vas-0
Vas-1
Vas-2
Vas-3
Vas-4
UMAP_2
UMAP_1
F
astrocyte
ependymal
microglia
OL lineage
vasculture
down
up
800
600
400
200
0
_subtype

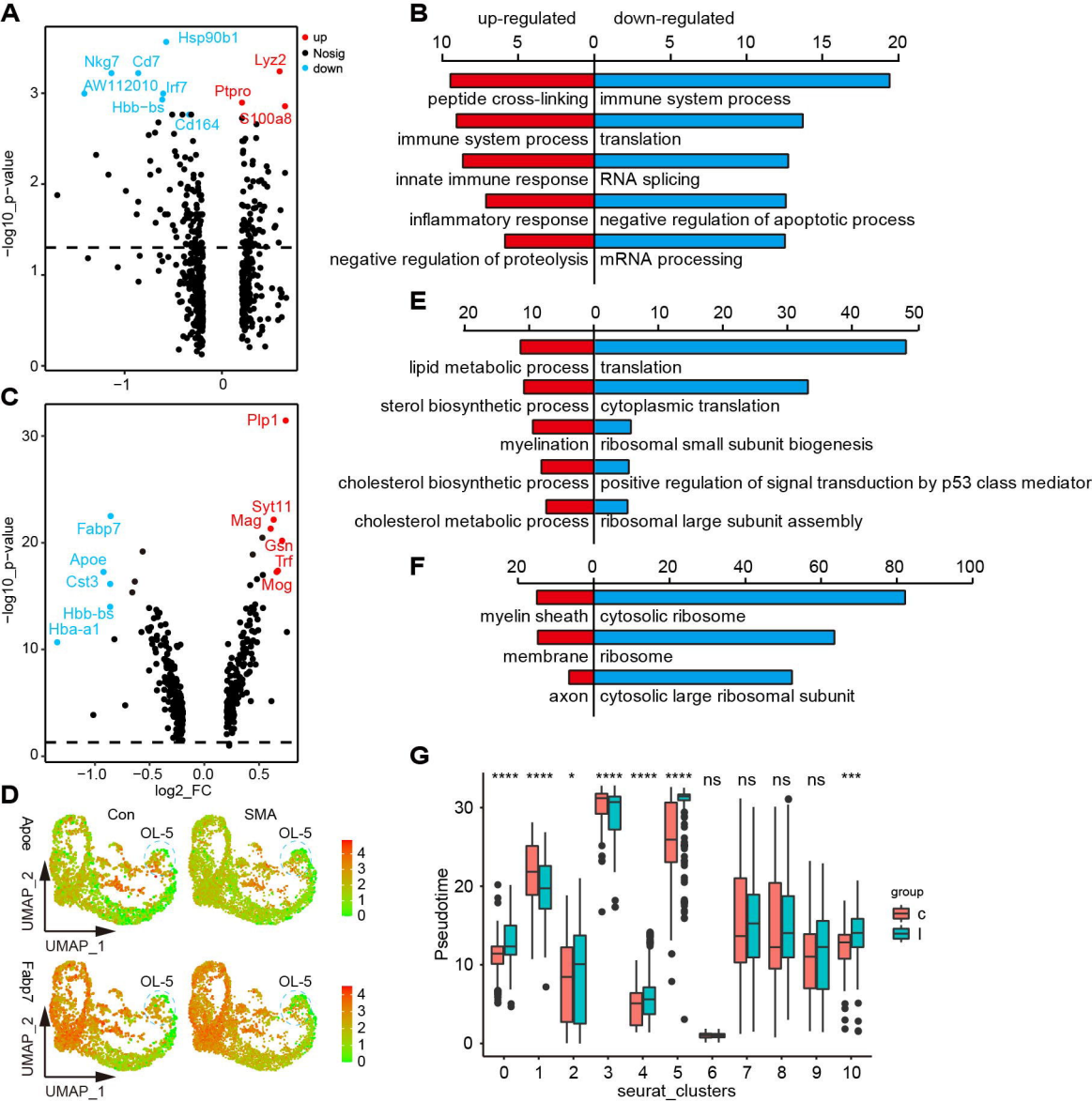
A
up
Nosig
down
Hsp90b1
Nkg7
Cd7
Lyz2
AW112010
Irf7
Ptpro
Hbb-bs
Cd164
S100a8
-log10_p-value
B
up-regulated
down-regulated
peptide cross-linking
immune system process
immune system process
translation
innate immune response
RNA splicing
inflammatory response
negative regulation of apoptotic process
negative regulation of proteolysis
mRNA processing
C
Plp1
Syt11
Mag
Fabp7
Gsn
Trf
Apoe
Cst3
Mog
Hbb-bs
Hba-a1
-log10_p-value
log2_FC
D
Con
SMA
Apoe
Fabp7
OL-5
UMAP_1
UMAP_2
E
lipid metabolic process
translation
sterol biosynthetic process
cytoplasmic translation
myelination
ribosomal small subunit biogenesis
cholesterol biosynthetic process
positive regulation of signal transduction by p53 class mediator
cholesterol metabolic process
ribosomal large subunit assembly
F
myelin sheath
cytosolic ribosome
membrane
ribosome
axon
cytosolic large ribosomal subunit
G
Pseudotime
seurat_clusters
group
C
I
ns
***

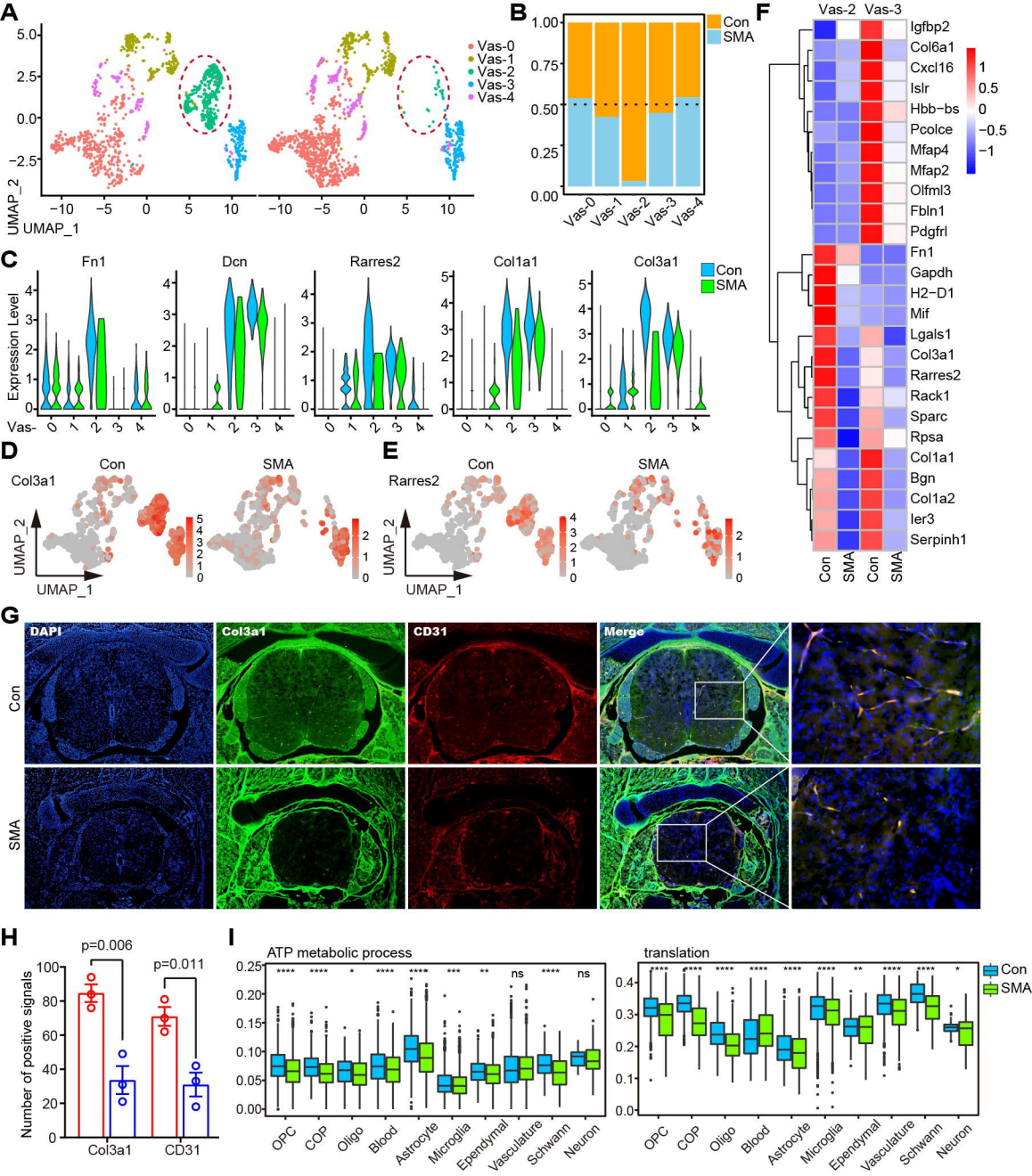
A
Vas-0
Vas-1
Vas-2
Vas-3
Vas-4
UMAP_1
UMAP_2
B
Con
SMA
Vas-0
Vas-1
Vas-2
Vas-3
Vas-4
C
Fn1
Dcn
Rarres2
Col1a1
Col3a1
Expression Level
Vas-
D
Col3a1
Con
SMA
E
Rarres2
F
Vas-2
Vas-3
Igfbp2
Col6a1
Cxcl16
Islr
Hbb-bs
Pcolce
Mfap4
Mfap2
Olfml3
Fbln1
Pdgfrl
Fn1
Gapdh
H2-D1
Mif
Lgals1
Col3a1
Rarres2
Rack1
Sparc
Rpsa
Col1a1
Bgn
Col1a2
Ier3
Serpinh1
G
DAPI
Col3a1
CD31
Merge
H
p=0.006
p=0.011
Number of positive signals
Col3a1
CD31
I
ATP metabolic process
translation
OPC
COP
Oligo
Blood
Astrocyte
Microglia
Ependymal
Vasculature
Schwann
Neuron

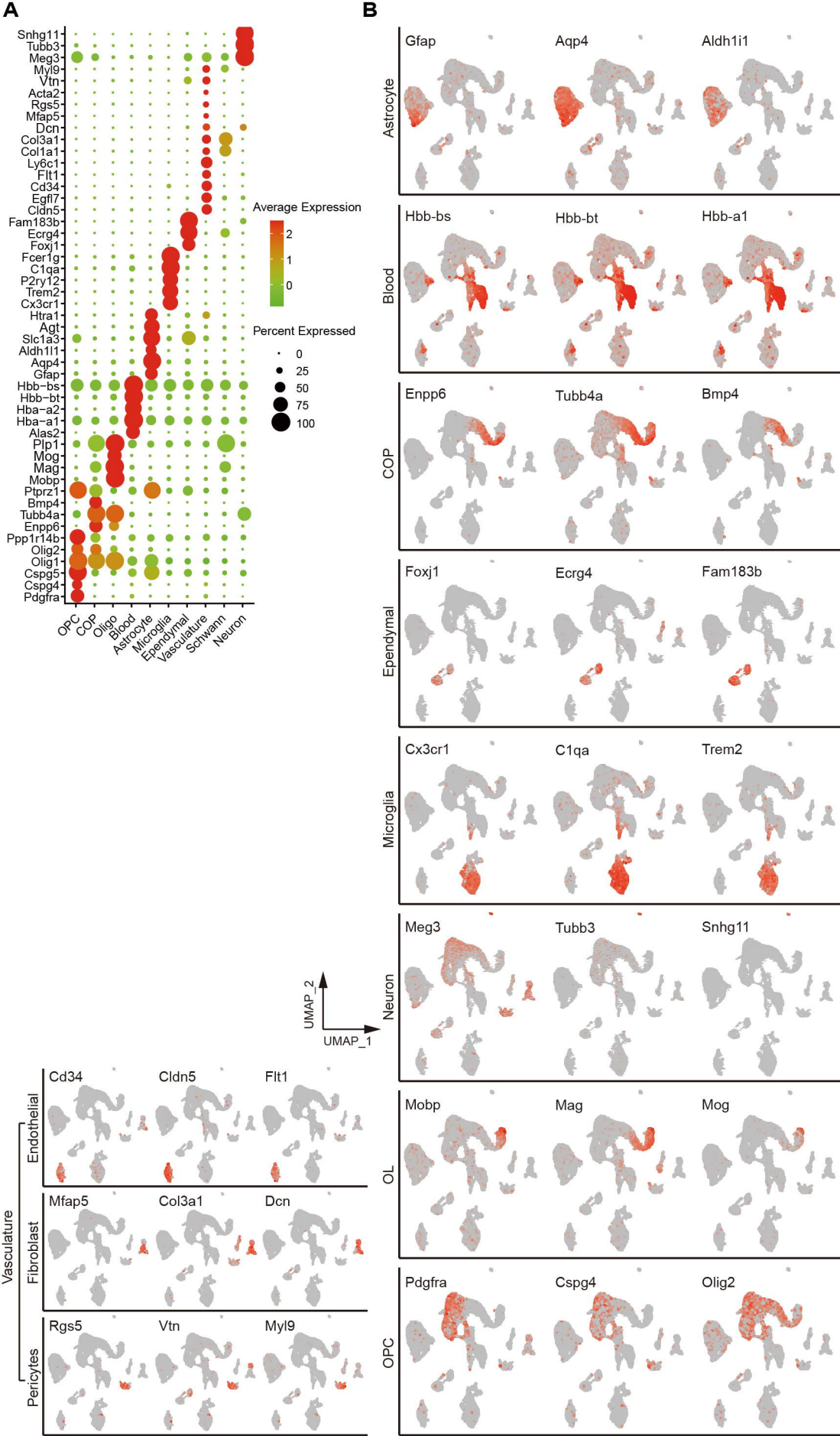
A
B
Snhg11
Tubb3
Meg3
Myl9
Vtn
Acta2
Rgs5
Mfap5
Dcn
Col3a1
Col1a1
Ly6c1
Flt1
Cd34
Egfl7
Cldn5
Fam183b
Ecrg4
Foxj1
Fcer1g
C1qa
P2ry12
Trem2
Cx3cr1
Htra1
Agt
Slc1a3
Aldh1l1
Aqp4
Gfap
Hbb-bs
Hbb-bt
Hba-a2
Hba-a1
Alas2
Plp1
Mog
Mag
Mobp
Ptprz1
Bmp4
Tubb4a
Enpp6
Ppp1r14b
Olig2
Olig1
Cspg5
Cspg4
Pdgfra
OPC
COP
Oligo
Blood
Astrocyte
Microglia
Ependymal
Vasculature
Schwann
Neuron
Average Expression
2
1
0
Percent Expressed
0
25
50
75
100
Astrocyte
Gfap
Aqp4
Aldh1i1
Blood
Hbb-bs
Hbb-bt
Hbb-a1
COP
Enpp6
Tubb4a
Bmp4
Ependymal
Foxj1
Ecrg4
Fam183b
Microglia
Cx3cr1
C1qa
Trem2
Neuron
Meg3
Tubb3
Snhg11
OL
Mobp
Mag
Mog
OPC
Pdgfra
Cspg4
Olig2
UMAP_2
UMAP_1
Vasculature
Endothelial
Cd34
Cldn5
Flt1
Fibroblast
Mfap5
Col3a1
Dcn
Pericytes
Rgs5
Vtn
Myl9

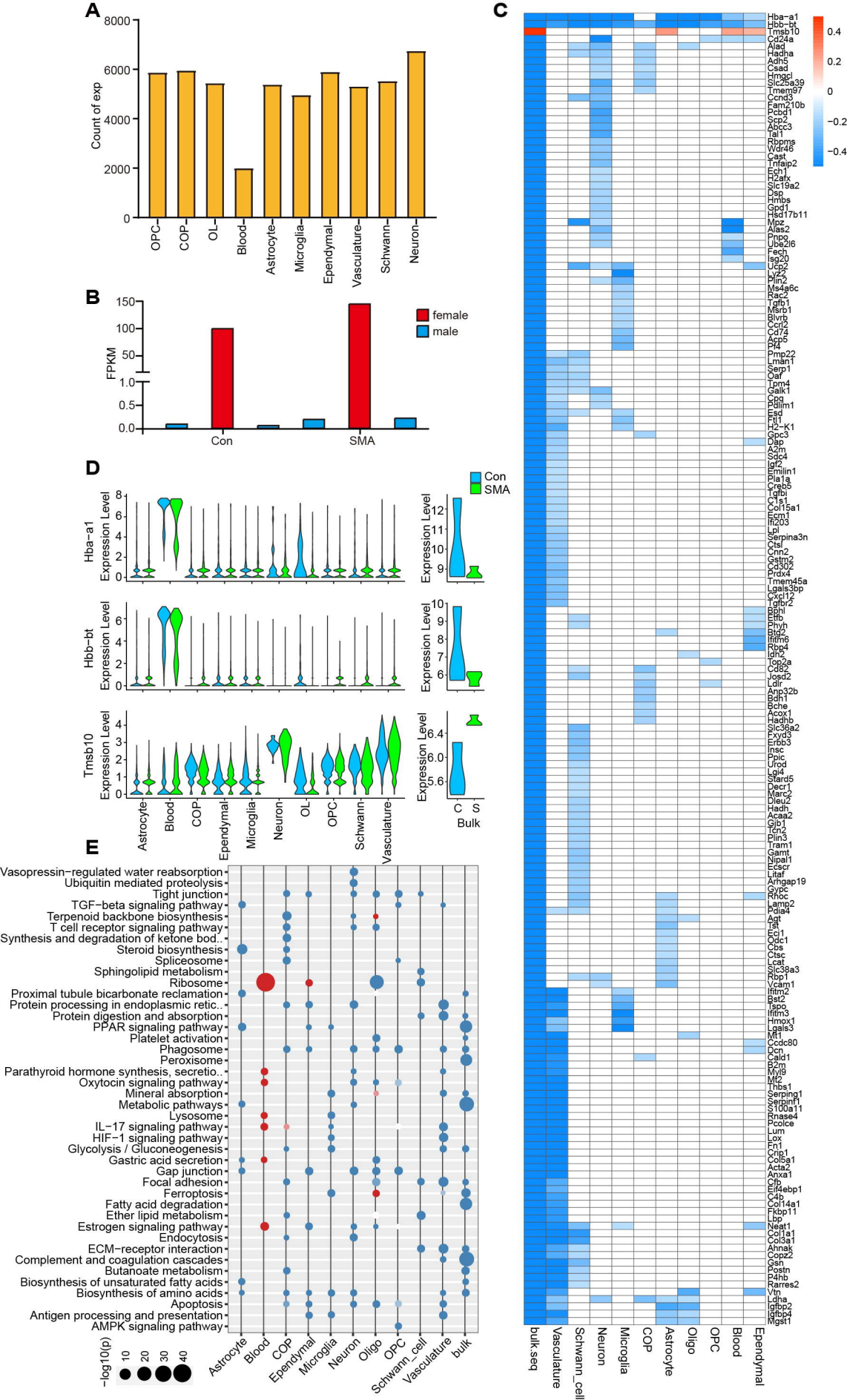
A
Count of exp
8000
6000
4000
2000
0
OPC
COP
OL
Blood
Astrocyte
Microglia
Ependymal
Vasculature
Schwann
Neuron
B
FPKM
150
100
50
1.0
0.5
0.0
female
male
Con
SMA
D
Con
SMA
Hba−a1
Hbb−bt
Tmsb10
Expression Level
Astrocyte
Blood
COP
Ependymal
Microglia
Neuron
OL
OPC
Schwann
Vasculature
C
S
Bulk
E
Vasopressin−regulated water reabsorption
Ubiquitin mediated proteolysis
Tight junction
TGF−beta signaling pathway
Terpenoid backbone biosynthesis
T cell receptor signaling pathway
Synthesis and degradation of ketone bod..
Steroid biosynthesis
Spliceosome
Sphingolipid metabolism
Ribosome
Proximal tubule bicarbonate reclamation
Protein processing in endoplasmic retic..
Protein digestion and absorption
PPAR signaling pathway
Platelet activation
Phagosome
Peroxisome
Parathyroid hormone synthesis, secretio..
Oxytocin signaling pathway
Mineral absorption
Metabolic pathways
Lysosome
IL−17 signaling pathway
HIF−1 signaling pathway
Glycolysis / Gluconeogenesis
Gastric acid secretion
Gap junction
Focal adhesion
Ferroptosis
Fatty acid degradation
Ether lipid metabolism
Estrogen signaling pathway
Endocytosis
ECM−receptor interaction
Complement and coagulation cascades
Butanoate metabolism
Biosynthesis of unsaturated fatty acids
Biosynthesis of amino acids
Apoptosis
Antigen processing and presentation
AMPK signaling pathway
−log10(p)
10
20
30
40
Astrocyte
Blood
COP
Ependymal
Microglia
Neuron
Oligo
OPC
Schwann_cell
Vasculature
bulk
C
Hba−a1
Hbb−bt
Tmsb10
0.4
0.2
0
−0.2
−0.4
bulk.seq
Vasculature
Schwann_cell
Neuron
Microglia
COP
Astrocyte
Oligo
OPC
Blood
Ependymal

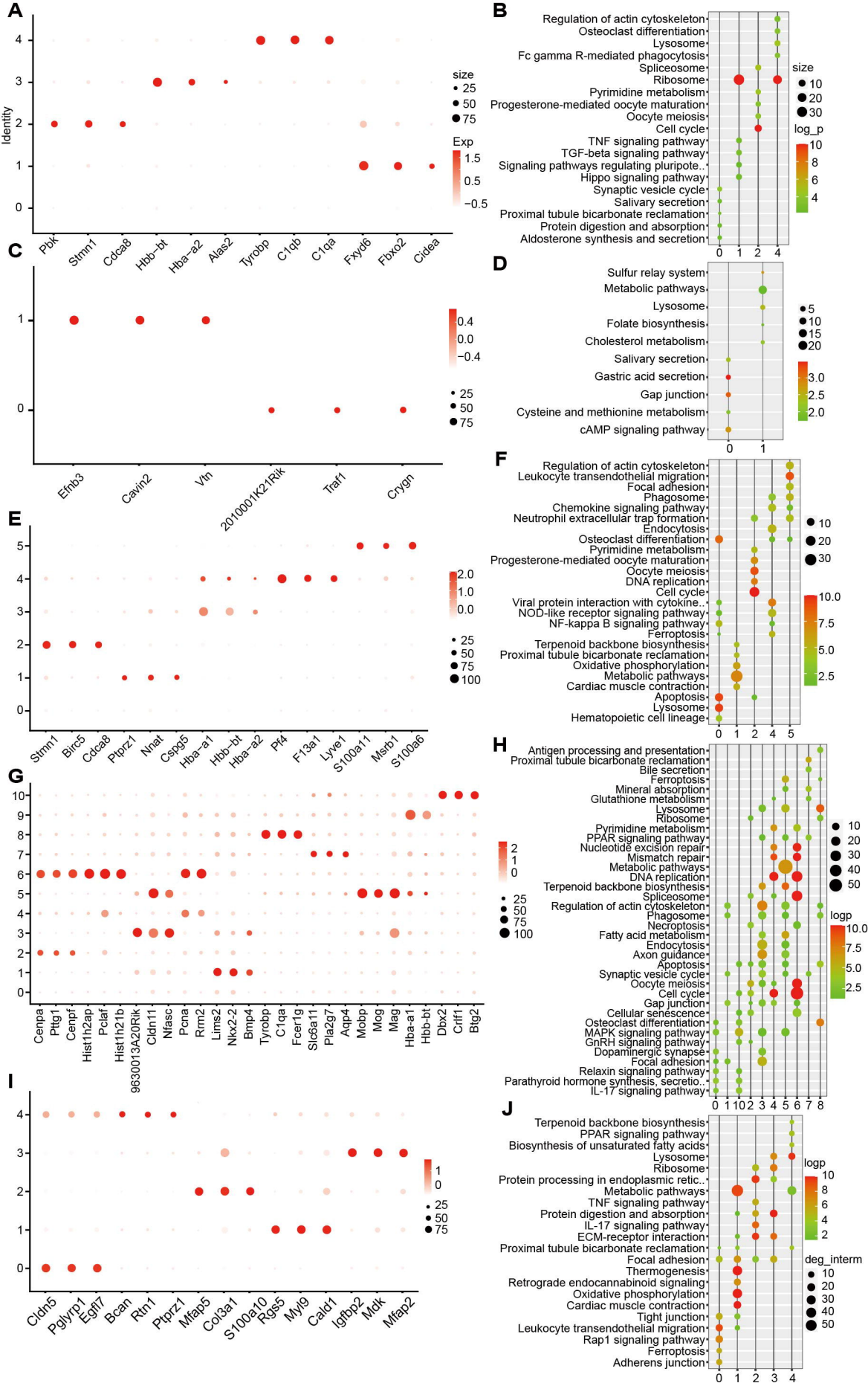
A
Identity
Pbk
Stmn1
Cdca8
Hbb-bt
Hba-a2
Alas2
Tyrobp
C1qb
C1qa
Fxyd6
Fbxo2
Cidea
size
Exp
B
Regulation of actin cytoskeleton
Osteoclast differentiation
Lysosome
Fc gamma R-mediated phagocytosis
Spliceosome
Ribosome
Pyrimidine metabolism
Progesterone-mediated oocyte maturation
Oocyte meiosis
Cell cycle
TNF signaling pathway
TGF-beta signaling pathway
Signaling pathways regulating pluripote..
Hippo signaling pathway
Synaptic vesicle cycle
Salivary secretion
Proximal tubule bicarbonate reclamation
Protein digestion and absorption
Aldosterone synthesis and secretion
size
log_p
C
Efnb3
Cavin2
Vtn
2010001K21Rik
Traf1
Crygn
D
Sulfur relay system
Metabolic pathways
Lysosome
Folate biosynthesis
Cholesterol metabolism
Salivary secretion
Gastric acid secretion
Gap junction
Cysteine and methionine metabolism
cAMP signaling pathway
E
Stmn1
Birc5
Cdca8
Ptprz1
Nnat
Cspg5
Hba-a1
Hbb-bt
Hba-a2
Pf4
F13a1
Lyve1
S100a11
Msrb1
S100a6
F
Regulation of actin cytoskeleton
Leukocyte transendothelial migration
Focal adhesion
Phagosome
Chemokine signaling pathway
Neutrophil extracellular trap formation
Endocytosis
Osteoclast differentiation
Pyrimidine metabolism
Progesterone-mediated oocyte maturation
Oocyte meiosis
DNA replication
Cell cycle
Viral protein interaction with cytokine..
NOD-like receptor signaling pathway
NF-kappa B signaling pathway
Ferroptosis
Terpenoid backbone biosynthesis
Proximal tubule bicarbonate reclamation
Oxidative phosphorylation
Metabolic pathways
Cardiac muscle contraction
Apoptosis
Lysosome
Hematopoietic cell lineage
G
Cenpa
Pttg1
Cenpf
Hist1h2ap
Pclaf
Hist1h21b
9630013A20Rik
Cldn11
Nfasc
Pcna
Rrm2
Lims2
Nkx2-2
Bmp4
Tyrobp
C1qa
Fcer1g
Slc6a11
Pla2g7
Aqp4
Mobp
Mog
Mag
Hba-a1
Hbb-bt
Dbx2
Crlf1
Btg2
H
Antigen processing and presentation
Proximal tubule bicarbonate reclamation
Bile secretion
Ferroptosis
Mineral absorption
Glutathione metabolism
Lysosome
Ribosome
Pyrimidine metabolism
PPAR signaling pathway
Nucleotide excision repair
Mismatch repair
Metabolic pathways
DNA replication
Terpenoid backbone biosynthesis
Spliceosome
Regulation of actin cytoskeleton
Phagosome
Necroptosis
Fatty acid metabolism
Endocytosis
Axon guidance
Apoptosis
Synaptic vesicle cycle
Oocyte meiosis
Cell cycle
Gap junction
Cellular senescence
Osteoclast differentiation
MAPK signaling pathway
GnRH signaling pathway
Dopaminergic synapse
Focal adhesion
Relaxin signaling pathway
Parathyroid hormone synthesis, secretio..
IL-17 signaling pathway
logp
I
Cldn5
Pglyrp1
Egfl7
Bcan
Rtn1
Ptprz1
Mfap5
Col3a1
S100a10
Rgs5
Myl9
Cald1
Igfbp2
Mdk
Mfap2
J
Terpenoid backbone biosynthesis
PPAR signaling pathway
Biosynthesis of unsaturated fatty acids
Lysosome
Ribosome
Protein processing in endoplasmic retic..
Metabolic pathways
TNF signaling pathway
Protein digestion and absorption
IL-17 signaling pathway
ECM-receptor interaction
Proximal tubule bicarbonate reclamation
Focal adhesion
Thermogenesis
Retrograde endocannabinoid signaling
Oxidative phosphorylation
Cardiac muscle contraction
Tight junction
Leukocyte transendothelial migration
Rap1 signaling pathway
Ferroptosis
Adherens junction
logp
deg_interm

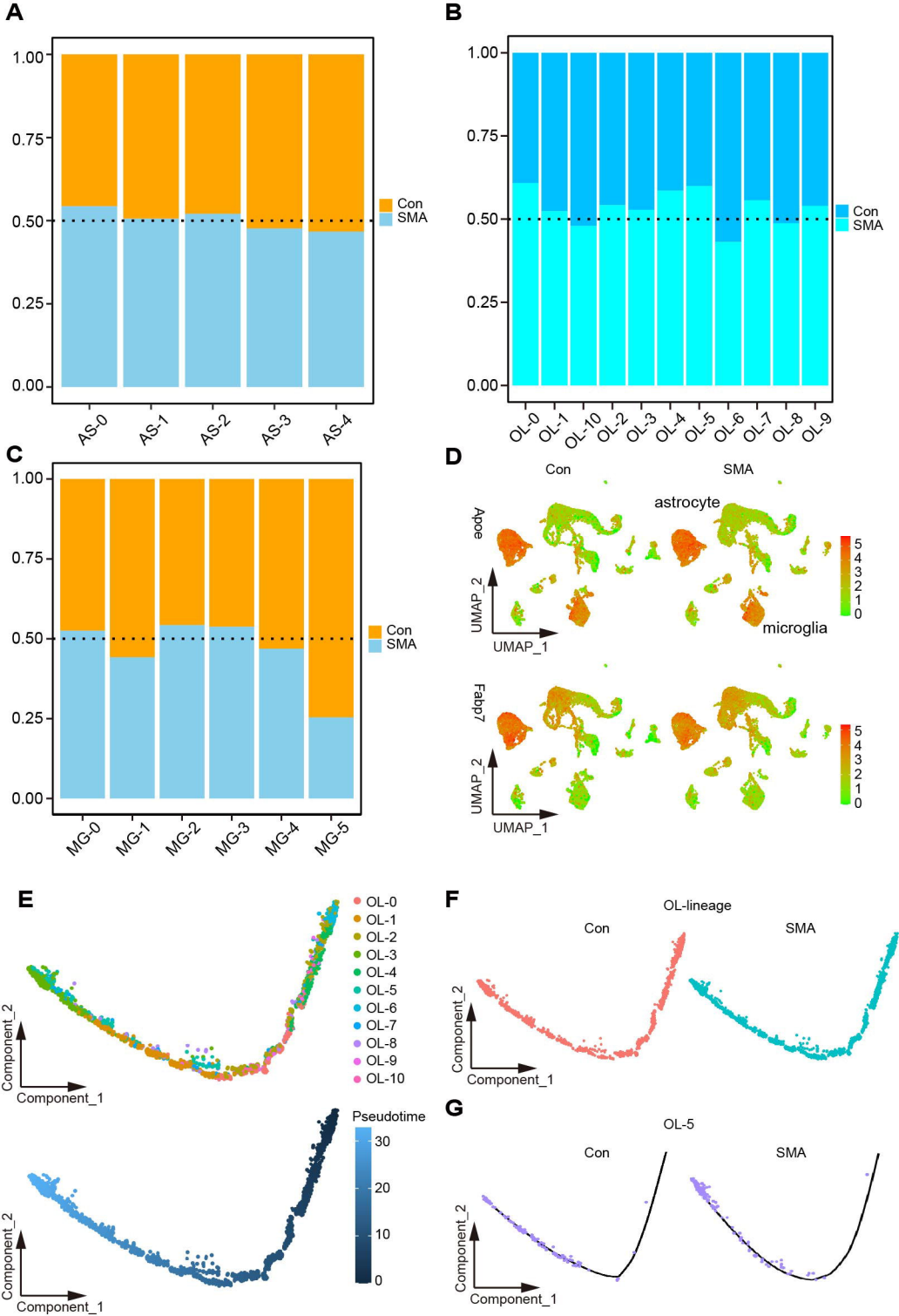
A
1.00
0.75
0.50
0.25
0.00
Con
SMA
AS-0
AS-1
AS-2
AS-3
AS-4
B
OL-0
OL-1
OL-10
OL-2
OL-3
OL-4
OL-5
OL-6
OL-7
OL-8
OL-9
C
MG-0
MG-1
MG-2
MG-3
MG-4
MG-5
D
Con
SMA
astrocyte
microglia
Apoe
Fabp7
UMAP_1
UMAP_2
E
OL-0
OL-1
OL-2
OL-3
OL-4
OL-5
OL-6
OL-7
OL-8
OL-9
OL-10
Component_1
Component_2
Pseudotime
F
OL-lineage
G
OL-5

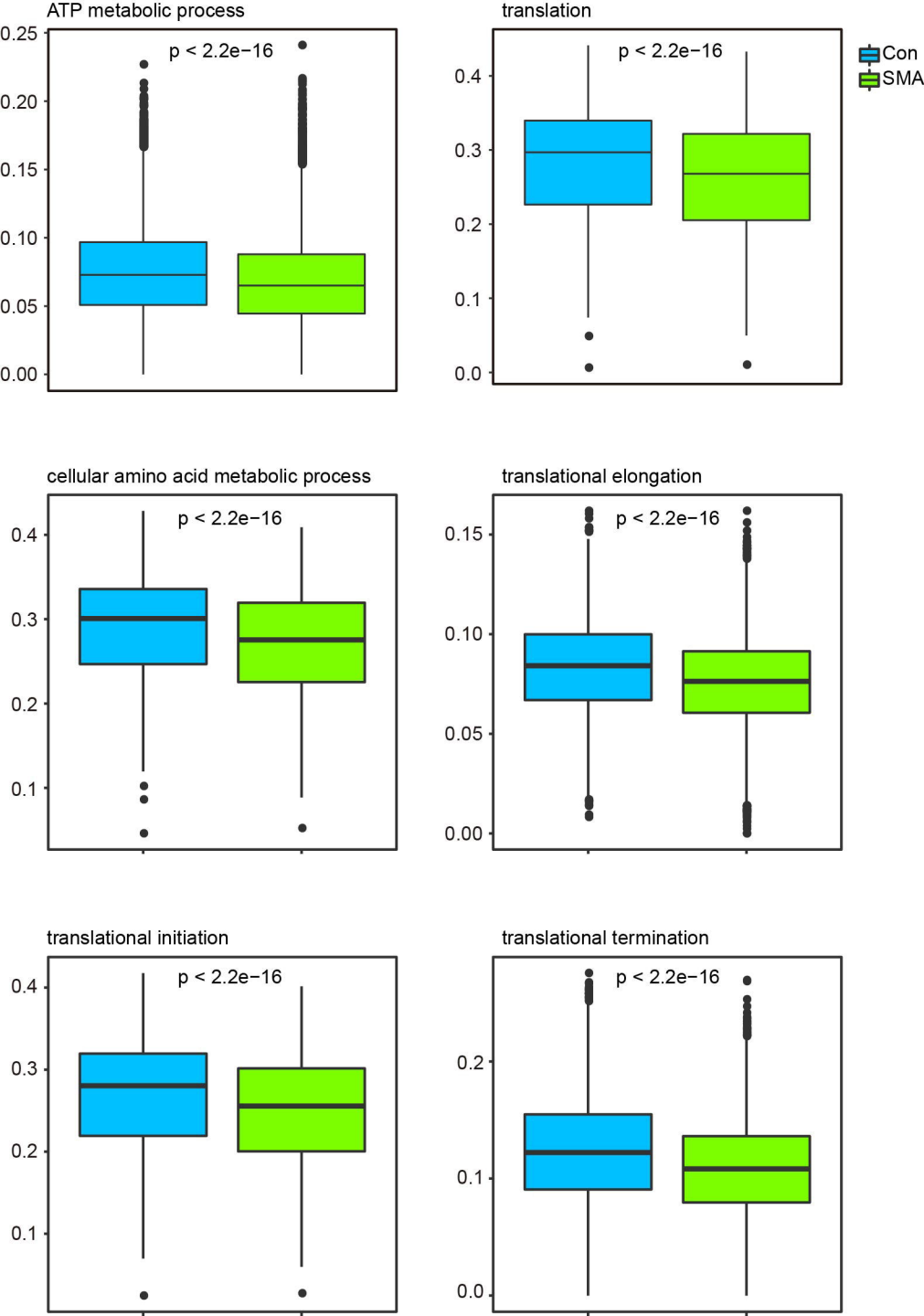
ATP metabolic process
p < 2.2e−16
0.25
0.20
0.15
0.10
0.05
0.00
translation
p < 2.2e−16
0.4
0.3
0.2
0.1
0.0
Con
SMA
cellular amino acid metabolic process
p < 2.2e−16
0.4
0.3
0.2
0.1
translational elongation
p < 2.2e−16
0.15
0.10
0.05
0.00
translational initiation
p < 2.2e−16
0.4
0.3
0.2
0.1
translational termination
p < 2.2e−16
0.2
0.1
0.0